Final Report

EOARD Contract # F61775-99-WE016

"High-power III-V mid-infrared lasers for the spectral range 3.0-3.6 μm"

Principal Investigator: *Yury P. Yakovlev, Dr. Sci., Prof,*

Director,
Scientific Engineering Center
For Microelectronics
of A.F.Ioffe Institute *Michail N. Mizerov, Ph.D.*

Work period: *12 months (June 1999-May 2000)*

SEC for Microelectronics of Ioffe Physico-Technical Institute
Saint- Petersburg
Russia

REPORT DOCUMENTATION PAGE

Form Approved OMB No. 0704-0188

1. AGENCY USE ONLY (Leave blank)	2. REPORT DATE	3. REPORT TYPE AND DATES COVERED
	2000	Final Report

4. TITLE AND SUBTITLE

High Power III-V Mid-IR Lasers for the Spectral Range of 3 - 3.6 Microns

5. FUNDING NUMBERS

F61775-99-WE

6. AUTHOR(S)

Dr. Yury Yakovlev

7. PERFORMING ORGANIZATION NAME(S) AND ADDRESS(ES)

SEC for Microelectronics of Ioffe Physico-Technical Institute
26 Polytechnicheskaya St
St. Petersburg 194021
Russia

8. PERFORMING ORGANIZATION REPORT NUMBER

N/A

9. SPONSORING/MONITORING AGENCY NAME(S) AND ADDRESS(ES)

EOARD
PSC 802 BOX 14
FPO 09499-0200

10. SPONSORING/MONITORING AGENCY REPORT NUMBER

SPC 99-4016

11. SUPPLEMENTARY NOTES

12a. DISTRIBUTION/AVAILABILITY STATEMENT

Approved for public release; distribution is unlimited.

12b. DISTRIBUTION CODE

A

13. ABSTRACT (Maximum 200 words)

This report results from a contract tasking SEC for Microelectronics of Ioffe Physico-Technical Institute as follows: The contractor will investigate high power mid-IR lasers based on III-V semiconductorheterostructures. Such lasers based on type I and IIInAs(Sb)/InGaAsSb, GaInAsSb/In(Ga)As(Sb) double heterstructures and also novel lasers with asymmetric band offset confinement will be fabricated and studied both theoretically and experimentally. Three samples of the type II lasers and three samples of the LED2 structures will be delivered at the end of the contract.

14. SUBJECT TERMS

EOARD, Diode lasers, semiconductor lasers, Mid-IR lasers

15. NUMBER OF PAGES

16. PRICE CODE

N/A

17. SECURITY CLASSIFICATION OF REPORT	18. SECURITY CLASSIFICATION OF THIS PAGE	19. SECURITY CLASSIFICATION OF ABSTRACT	20. LIMITATION OF ABSTRACT
UNCLASSIFIED	UNCLASSIFIED	UNCLASSIFIED	UL

Key persons:

Maya P. Mikhailova, Deputy P.I., Dr.Sci., p.r.s.
Albert N. Imenkov, Dr.Sci., l.r.s.
Andrei M.Monakhov, Ph.D., s.r.s.
Sergei V. Ivanov, Ph.D., s.r.s.
Georgy G. Zegrya, Dr.Sci., Prof.
Konstantin D. Moiseev, Ph.D., r.s.
Boris A. Matveev, Ph. D., s.r.s.

Investigators:

Boris Ya. Meltzer, Ph.D., s.r.s.
Victor A. Solovjev, Ph. D., s.r.s.
Victor V. Sherstnev, Ph.D., s.r.s.
Michail V. Stepanov, j.r.s.
Anastasia P. Astakhova, postgrad.
Vladimir A. Druzhinin, chief eng.
Tatyana I. Kachalova, secr.

p.r.s. - principal research scientist
l.r.s. - leading research scientist
s.r.s. - senior research scientist
r.s. - research scientist
j.r.s. - junior research scientist

Content.

1. Introduction

Recently, mid-infrared semiconductor lasers have received a great deal of attention for potential application in atmospheric trace monitoring, common pollutant analysis, and ultra-loss optical fiber communication. For most of these applications, reliable high power operation is of great importance. Continuous wave operation of these lasers in combination with high frequency modulation techniques is important in high-resolution laser diode spectroscopy. Since the signal to noise root of the laser power is proportional to square root of the laser power on the detector[1], so the cw output power should be as high as possible. But high optical power in a single cw mode is still a problem.

III-V compound lasers based on InAsSb, InAs/GaInSb operating in the spectral range of 3-4μm can now reach high peak optical power in pulsed mode up to 1-4W at 80K[2-4] and up to 2-10mW in the cw mode at 80-100K[5]. They have a great advantage over the lead salt lasers whose maximum output power is typically less than 1mW in multi-mode operation and in cw mode their optical power is below 300μW[6].

Unfortunately, the performance of the narrow-gap III-V semiconductor lasers is strongly influence by non-radiative Auger-recombination process, intervalence band absorption, carrier heating and carrier leakage effect. Hence, to solve high-power mid-ir diode laser problem the theoretical consideration of above mentioned processes requires as well as experimental verification of conventional type I and type II structures based on arsenide/antimonide compounds.

Now some new physical approaches and new band gap engineering are necessary to design laser structures where loss processes are suppressed. It can be achieved in laser structures combining advantages of type I and type II heterostructures. It is known that weak wave function overlapping at the interface in the type II heterostructures leads to decreasing quantum efficiency and the lower optical power in comparison to type I lasers. On the other side, it have been predicted that Auger losses can be significantly suppressed in the type II heterojunctions[7,8]. It allows to get higher peak output power as well as weaker temperature dependence of the threshold current But intravalence band absorption and carrier heating processes do not considered enough up to day theoretically for narrow-gap III-V lasers based on InAs alloys[9]. However, it is known that carrier heating plays a great role in InAs and InSb based materials, especially at high injection level or at low temperatures. Besides, the increasing of laser output power can be reached by the optimization of the broad-waveguide of the laser[11,12].

There are several ways to realize high-power III-V narrow-gap lasers. One of them consists in optimization of main parameters of the conventional type I and type II InAsSb/InAsSbP and GaInAsSb/InGaAsSb lasers, in according to theoretical calculations. The second way is to use a new physical approach to the band gap engineering of the novel laser structure which can combine some advantages of type I and type II lasers and provide the higher optical gain, higher quantum efficiency, and where carrier heating and current leakage processes are excluded.

In this work we report a new physical approach for the design of laser structure with strong, asymmetric band offset confinements to improve power and temperature characteristics of the mid-ir devices. Conventional type I and type II laser structures based on In(Ga)AsSb/InAsSbP DH were grown by LPE on InAs(100) and (111A) and fabricated with broad-area stripes (100-200 μm). We succeeded in achievement of optical power up to 1W in pulsed mode at λ=3.2-3.6 μm (T=80-120K). Characteristic temperature T=49-60K was obtained at T=80-180K for the type II near-broken gap laser structure based on GaInAsSb/InGaAsSb/InAsSbP. Some results of MBE growing and study of multiquantum wells and short-period superlattices based on GaSb/InAs/AlSb, InAs/GaSb, AlGaSb/GaSb are presented. Special attention was paid to growing MBE structures with high quality interface[18,19]. These MQW are basic structures for further growing of a new mid-IR laser with asymmetric band offset confinement.

Finally, a novel hybrid III-V/II-VI double heterostructure AlSbAs/InAs/Cd(MgSe) was proposed and grown for the first time by original two-stage MBE technology method as prospective model for a new asymmetric mid-ir-laser.

2. Summary

A new physical approach have been proposed in the frame of the Proposal to band-gap engineering of mid-infrared laser design which allows to reach higher optical power, higher quantum efficiency and weaker its temperature dependence. Asymmetric heterostructure with large band offsets for electrons ΔE_c and holes ΔE_v was theoretically proposed and realized combining some advantages of type I and type II heterostructures.

Physical model of a new laser design was considered and a suppression of the injection current losses was predicted.

Several types of III-V based laser structures were fabricated by LPE and study: type I In(Ga)AsSb/InAsSbP DH lasers grown on InAs (100) and (111A) substrates operating in the spectral range 3.2-3.4 μm, type II GaInAsSb/InGaAsSb/InAsSbP DH lasers grown on p-InAs (100) substrates operating at λ=3.26 μm (77K) and type II AlGaAsSb/InGaAsSb DH laser with high asymmetric band offsets operating at λ=3.2-3.8 μm at 77K. Theoretical calculation and simulation of intravalence band absorption in type I InAsSb/InAsSbP heterolaser with taken into account spin-orbit splitting valence band was performed. Comparative study of spontaneous and coherent spectra, current-output power characteristics, differential quantum efficiency and temperature dependence of the threshold current was made.

High-power broad-area (L=350 μm d=100-200 μm) mid-infrared lasers based on InGaAsSb/InAsSbP DH with Cd doped active layer were fabricated and pulse output power over 1W was achieved for the first time.

Type II asymmetric GaInAsSb/InGaAsSb/InAsSbP laser structures demonstrated up to 0.75 mW in pulse mode (d=90 μm) and 20 mW in cw mode.

Some results of MBE growing of multiquantum wells InAs/GaSb/AlSb and short-period superlattices GaAsSb/InAs/GaSb/GaSb were presented together with photo- and electroluminescence data. Intense electroluminescence was obtained from InAs/GaSb/AlSb light-emitting diodes at 77 and 300K. Novel technical and band-gap engineering approach was suggested also to make laser structures with large band offsets for electrons and holes by using growing of hybrid heterostructure II-VI on II-V materials (dSe and d(Mg) Se were chosen for this purpose.We have fabricated the first hybrid AlSbAs/InAs/(d(Mg)Se heterostructure by MBE, consequently in two separate grown chambers. Photo- and electroluminescence at λ>3 μm were observed in the structure both at low (77K) and room temperature. Weak temperature dependence of quantum efficiency was obtained. New proposed structure is very promising to design of novel type high-power mid-ir lasers.

3. Program Objective

The main objective of this one year proposal is realization and study of high-power III-V mid-infrared lasers operating in cw (quasi-cw) and pulsed mode.

To solve main goal of the Proposal the following practical tasks will be carried out:

1. Fabrication and study of high-power laser structures based on type I and type II heterojunctions in the InAsSb/InAsSbP and GaInAsSb/In(Ga)As(As) systems grown by LPE method will be performed. Mesa-stripe (both narrow-stripe and broad-area) lasers operating in cw mode and in pulsed mode (single mode and multi-mode operation) will be made.
2. Theoretical calculation and simulation of main processes limiting high-power and high-temperature operation of III-V mid-IR diode lasers will be carried
3. Novel multi-quantum well laser structures with asymmetric band offset confinement on the base of GaAs(Sb)/InAs/InP system will be proposed to fabricate by MBE.
4. Theoretical model of the asymmetric laser structure will be proposed. Advantages of such laser model in comparison with both type I and type II heterostructures will be demonstrated.
5. Multi-quantum wells and short period superlattices based on InAS/GaSb/AlSb, AlSb/GaSb and InAs/GaSb will be grown by MBE method and PL and EL study will be performed.
6. Novel physical and technological approach for design of mid-ir laser structure with high asymmetric band offset confinement with using hybrid III-V/II-VI MBE grown heterostructure will be proposed.
7. Comparative investigation of the three laser structures will be made (current-voltage and power-current characteristics, differential quantum efficiency, spontaneous and coherent emission, temperature dependence of the threshold current etc.). Optimization of the laser structures for high power operation will be proposed.

Main results of the project will be the realization of high-power mid-ir lasers for the spectral range 3-3.6 μm including narrow-stripe single mode cw or quasi-cw lasers with the optical power up to 10-20 mW and multi-mode broad-area pulsed lasers operating near room temperature or by TE-cooling with peak power up to 1W. A new model of laser with strong asymmetric band offset confinement will be also demonstrated.

4. Technical Schedule

I quarter (June, July, August 1999)
Fabrication of III-V laser structures
1. Epitaxial growing of laser heterostructures type I and type II in the systems of InAsSb/InAsSbP and GaInAsSb/In(Ga)As(Sb) by LPE method.
2. MBE growing quantum well laser structures with asymmetric band offset confinement on the base of GaAs(Sb)/InAs/InP.
3. X-ray diagnostics of laser structures, EBIC control (electron beam induced current)

II quarter (September, October, November 1999)
Theoretical and experimental study of the laser performance
1. Theoretical calculation and simulation of the processes limiting high optical power and high temperature operation of mid-ir laser structures (Auger-recombination, interavalence band absorption, carrier heating)
2. Fabrication of mesa-stripe laser structures with narrow stripe (d=10μm) and broad area (d=100-200μm).
3. Experimental study of spontaneous and coherent emission, current-voltage characteristics, differential quantum efficiency and temperature dependence of the threshold current at 77-300K for the InAsSb/InAsSbP and GaInAsSb/InGaAsSb lasers grown by LPE.
4. Experimental study of the electroluminescence in quantum-well laser structures, grown by MBE.

III quarter (December 1999, January, February 2000)
Comparative study of the optical power for the three kinds of the laser structures
1. Investigation of optical power and power-current characteristics in the InAsSb/InAsSbP and GaInAsSb/In(Ga)As(Sb) laser structures in the cw and quasi-cw mode.
2. Investigation of the peak optical power of the laser structures under study in pulsed mode.
3. Comparative analysis of calculated and experimental laser performances and determination of the main factors limiting optical power and high temperature operation.

IV quarter (March, April, May 2000)
1. Theoretical investigation of the heating processes (carrier heating, thermoionic emission, Jouly heating) in the high-power mid-ir lasers under study.
2. Comparative study of the high-power and the temperature characteristics of the three kinds of laser designs.
3. The recommendation for the design optimization of the high-power mid-infrared laser structures.

5. Theoretical model of an asymmetrical laser structure with high band offsets.

New physical concept is in using asymmetrical heterostructure with high band offsets at the interface between an active layer and wide gap confined layers. In this structure a narrow active layer (quantum well or superlattice) sandwiched between wide-gap layers forming type I heterojunction (Fig.1). Wide gap n- and p-layers form type II heterojunction pairs and have Eg higher than photon energy of emission.

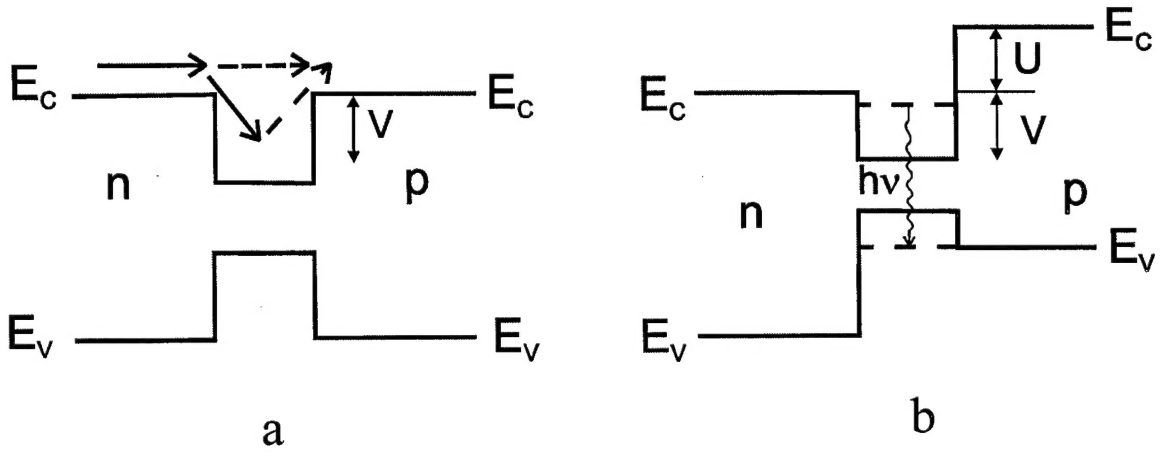

Fig.1. Energy band diagram of mid-infrared laser structure for standard DH-structure (a) and the structure with asymmetric band-offset confinement (b).

In this model asymmetric quantum well is the main feature of new laser. Optical confinement will be made by using wide gap thicker layers (2-3 μm) based, for example, on InAsSbP or GaInAsSb. In such heterostructure a strong wave functions overlapp wave functions of electrons and holes at the heteroboundary with an active layer takes place. It leads to the same optical gain as it is in traditional double heterolasers, but by substratial suppression both injection and non-radiative losses. In proposed device a low threshold current and its weak temperature dependence are expected.

As compared to standard type I heterostructure shown in Fig. 1a, new asymmetric structure (Fig. 1b) allows to reduce operation current of the laser. Indeed, total current is sum of radiative (non-radiative) recombination and drift (injection) component. Recombination currents should be the same in the active region of both structures. But as to leakage currents their ratio will be

$$\frac{J_1}{J_2} \approx \exp\left(-\frac{U}{kT_{eff}}\right), \qquad (1)$$

where J_1, J_2 are total current for the structure shown in Fig. 1a and Fig. 1b respectively, T_{eff} is effective temperature of an active layer, and V is height of barrier. This current is not high in comparison with recombination current at low temperature and low optical power.

The threshold current is $J_{th}=J_R+J_{leak}$, where J_{leak} is the leakage current which consists of non-radiative recombination current, Auger-current and injection losses which are due to the carriers injection from the quantum well to n- and p-regions:

$$J_{leak} = J_{NR} + J_A + J_{inj}. \qquad (2)$$

If the height of the energy barriers U_1 and U_2, that is equal to $(E_{CR}-E_{CN})$ for electrons and $(E_{VN}-E_{VP})$ for holes respectively, are chosen to exceed 3-5 kT at working temperature of the device (200-300K), the last term in the expression for the leakage current can be neglected and the total current is determined only by the recombination one in the narrow-gap region of device. It can be called "non-injection" current, because no current injection through p-n junction occurs. The calculations of the Auger-recombination losses carried out for type II heterojunction[7], which can be used as an estimation for our case, shows that proposed device provides at least the 25 times higher gain in the laser structure with asymmetric band offset confinement (ABOC) with respect to that in a conventional type I heterojunction laser but at the same very low level of the injection losses. The proper QW material selection allows one to reduce also the Auger recombination losses by tuning out of a resonance between the photon energy and the energy gap to a spin-orbit splitted valence band.

Such a unique combination of the advantages of type I and type II heterostructure lasers in one QW ABOC laser structure allows us to believe that the novel ABOC laser under consideration will be able to operate at room temperature at the wavelength in the 3-6 μm range.

The advantages of the proposed QW ABOC laser in comparison with a quantum cascade laser are:

- the higher output power,
- the relative simplicity of fabrication,
- the ability to make a set of lasers for different wavelengths using the same technology and varying the QW width only.

To obtain laser generation a high density of states needs. To reach high power it is important to get real large density of generating centers.

To optimize laser performance, it needs:

1) to reduce of optical losses (for example, by using external resonator). Maximum output power begins to rise linearly with cavity length:

$$P_{output}^{\max} \equiv \alpha_0 l \left(1 - \sqrt{\frac{\beta}{\alpha_0}}\right)^2 P_S \qquad (3)$$

at reflector transparency

$$T_{opt} = 2\alpha_0 l \left(\sqrt{\frac{\beta}{\alpha_0}} - \frac{\beta}{\alpha_0}\right) \qquad (4)$$

2) to reduce electrical losses

3) to reduce non-radiative recombination losses and losses on non-coherent emission (quality of laser structures)

Then "ideal" laser structure must look as the following:

1. Low-dimensional active layer (quantum well, superlattice) with big number of homogeneous emitters.
2. Good optics in design of laser structure (resonators, indices)
3. Decreasing of injection current losses in an active layer.

This approach needs a careful theoretical calculation of the active region parameters to provide an existence of at least one well confined bound state for both types of the carries (electrons and holes) in the QW with asymmetric barrier heights. On the other hand, it is necessary to choose the materials for both the active and confining layers which should be able to form nearly lattice-matched heterostructure and to be grown by the currently available technological equipment (MBE, LPE, MOCVD).

The tentative calculation in a rectangle barrier approximation and not taking into account the complex valence band structure shows that the ABOC device based, for instance, on p-GaAsSb/InAs/n-InP or p-GaAsSb(Al)/InAsSb/n-InAsSbP heterostructures can operate at the room temperature at the wavelength of about 3 μm. These structures can be fabricated either by MBE, by LPE, MOCVD, or by MBE in combination with LPE technology.

5.1. Suppression of the injection current losses an asymmetric laser structure

Lets consider and compare an ideal model of the conventional laser double heterostructure (Fig.1a) and asymmetric structures (Fig. 1b). For simplicity we will consider the active region of both structures to be the same. Besides, we will suppose that the thickness of an active region is large enough (about 1 μm) as it is usual for LPE grown

structures. In this case we can use the quasi-classical approximation and neglect the quantum-size effects in the active layer.

Let's examine processes in the conduction band (similar processes take place in the valence band). Electrons which fall into an active region from n-region will relax by energy and captured in it, recombining then with holes (radiative or non-radiative), or leaving an active region by activation process. The difference between Fig.1a and Fig.1b is an existence of an additional barrier on the heterointerface of the region with another conductivity type. Such barrier firstly increases to some extent the carrier capture probability by active region due to an existence of a turn-off point at the classical trajectory near the barrier, but it is not very important because the capturing time is small enough even without this barrier. Secondly this barrier reduce the probability of carrier in injection from the active layer to the region with the inverse type of conductivity. The last process is more important and we will consider it in more details. Usually the energy relaxation time is much smaller than the radiative recombination time. Therefore, for our estimation we will suppose that there is the quasi-equilibrium in side an active region, with some characteristic temperature T and quasi-Fermi level coinciding approximately to band edge. Further, we suppose that carrier distribution in an active region is usual Fermi distribution. Then energy carrier density (number of carrier divided on the energy interval in the volume unit of an active layer) is:

$$dn(E) = \frac{\sqrt{2}\ m^{3/2}}{\pi^2\hbar^3} \cdot \frac{\sqrt{E}\ dE}{e^{\frac{e-\mu}{kT}} + 1} \qquad (5)$$

and the connection between the total average carrier density and the Fermi-level position is:

$$\bar{n} \equiv \frac{N}{V} = \frac{\sqrt{2}\ (mT)^{3/2}}{\pi^2\hbar^3} \int_0^\infty \frac{\sqrt{z}\ dz}{e^{z-\frac{\mu}{kT}} + 1} \qquad (6)$$

Injection losses are determined by the number of electrons, which go out to the right side from an active layer (See Fig 1). (Electrons going away to the left, in the n-region, are compensated by a proper number of coming electrons and do not contribute in the current in the device). At the same time electrons, which were injected into the p-region, can recombine and thus make some contribution to the total current). A number of such electrons in a time unity will be for the case in Fig. 1a:

$$J_{inj}^{(a)} = \frac{m^{3/2}}{\sqrt{2}\ \pi^2\hbar^3} \int_0^\infty \frac{\sqrt{x+V}\ dx}{e^{\frac{x}{kT}} + 1} \qquad (7)$$

And for the case in Fig. 1b,

$$J_{inj}^{(b)} = \frac{m^{3/2}}{\sqrt{2}\ \pi^2\hbar^3}\int_u^{\infty}\frac{\sqrt{x+V}\ \ dx}{e^{\frac{x}{kT}}+1} \qquad (8)$$

The ratio of these values (3) and (4) will be named efficiency β (T,U,V_0) of the injection suppression of the losses (b):

$$\beta(T,U,V) = 1 - \frac{\int_U^{\infty}\frac{\sqrt{x+V}}{e^{\frac{x}{kT}}+1}dx}{\int_0^{\infty}\frac{\sqrt{x+V}}{e^{\frac{x}{kT}}+1}dx} \qquad (9)$$

Fig.2a shows the temperature dependence of the function $\beta(T,U,V)$. It is evidently that although the injection efficiency decreases with temperature increase, but an injection suppression coefficient is still about 0.6 at room temperature. Now we evaluate decreasing of critical current of devices represented on Fig.1b in comparison with Fig.1a. We present the "pessimistic" estimation of the minimum profit in a critical current, which can be obtained due to additional barriers at the heteroboundary. Let's consider that all carrier with energies lying lower the Fermi level recombined with the same recombination time as carrier inject time over the barrier edge. This hypothesis leads to overestimation of the recombination current, but it is useful as the estimation of the ratio of the injection and the total current. Fig.2b inhibits the temperature dependence of this J_{inj}/J_{tot} ratio. It can be seen that injection current is about 30% from the total current, and using a Fig.1b design allows to reduce a threshold current at least by 20% at room temperature. In the same way some other sufficient values can be easily estimated. In Fig.2b it is shown the temperature dependence of the J_{inj}/J_{tot} ratio for device presented in Fig 1a. Fig.2c shows the same ratio as a function of the quantum well depth at T=300K. At last, in Fig. 2d and Fig.2e we plot the dependence of the efficiency of the injection current suppression as a function of value U and V. Our estimations show that proposed laser structures with asymmetric band offset confinements are effective especially under the following conditions:

a) High operation temperature;
b) b) Additional band offsets are about 2-3 kT;

c) c) Quantum well for carriers is not very deep. In this sense for the band offset of 30 meV in the valence band the injection suppression can be rather effective than for the band-offset in the conduction band of 200 meV.

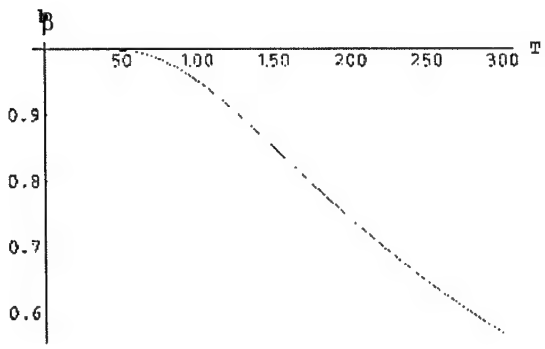

a

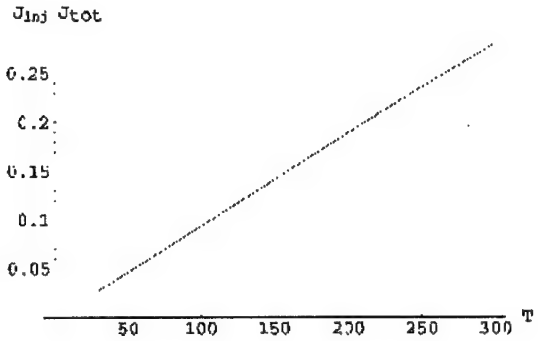

b

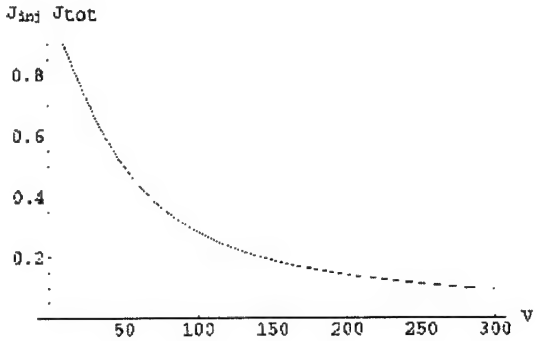

c

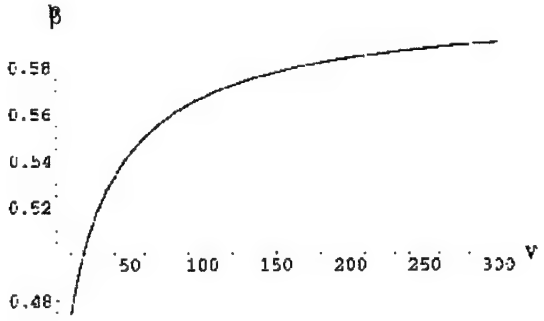

d

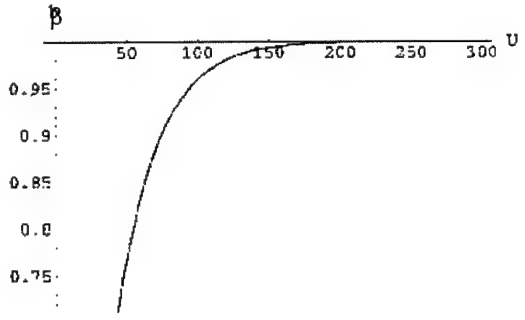

e

Fig.2 a) The temperature dependence of the injection current suppression for design in Fig 1b with U=100meV and U=30 meV. b) The temperature dependence of the ratio of the injection current to the total current for the design in Fig.1a with V=100meV. c) The dependence of the Jinj/Jtot on well depth design in Fig. 1a at T=300K. d) The dependence of the efficiency of injection current suppression of the well depth V for the

structure in Fig.1b with U=30meV at T=300K. e) The efficiency of injection current suppression as a function of the barrier heigh U for the structure in Fig.1b with v=100 meV at T=300K.

6. Epitaxial growing of type I and type II laser structures in the system In(Ga)AsSb/InAsSbP by LPE.

Type I and type II laser structures based on In(Ga)AsSb/InAsSbP, GaInAsSb/InGaAsSb and GaInAsSb/AlGaAsSb were grown by LPE lattice-matched on InAs substrates. The laser structures were controlled by X-ray diagnostics to determine a composition of solid-solutions (In(Ga)AsSb, InAsSbP, GaInAsSb). P-n junction location in the narrow-gap laser structures under study was controlled by electron beam induced current (EBIC) method[20].

6.1. Type I InAsSb/InAsSbP double heterostructure laser grown by LPE on InAs(100) substrate.

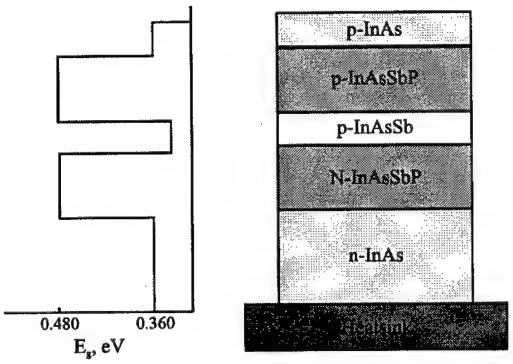

Fig.3. Schematic type I InAsSb/InAsSbP laser double heterostructure.

Lasers were fabricated from double heterostructures as shown in the schematic diagram of figure 1 and were grown from indium-rich melts by LPE[21]. Aconventional multi-well graphite sliding boat was used for the LPE growth of the LD structures. Epitaxy was carried out with the boat inside a high-purity quartz reactor tube in a flowing purified hydrogen gas atmosphere provided from a Pd-diffusion unit.

The resulting epitaxial structure was a double-heterostructure in which the unintentionally doped n-$InAs_{0.95}Sb_{0.05}$ active layer is enclosed between p-type and n-type $InAs_{0.42}Sb_{0.2}P_{0.44}$ confinement layers respectively. The P content in the confinement layers was 0.44 (Eg=578 meV, T = 77 K) so as to provide a higher bandgap energy and large interface band offsets for good carrier confinement. The $InAs_{0.95}Sb_{0.05}$ active region was 0.7 μm thick (Eg=344 meV, T = 77 K) and had a small lattice mismatch ($\Delta a/a$ =+0.35%) to the $InAs_{0.42}Sb_{0.2}P_{0.44}$ layers which themselves were iso-periodic with InAs and each 3.0 μm in thickness. As shown in figure 1 the

$InAs_{0.95}Sb_{0.05}/InAs_{0.42}Sb_{0.2}P_{0.44}$ heterostructure is type I in nature and so recombination would be expected from the $InAs_{0.95}Sb_{0.05}$ bulk. In order to obtain epitaxial material of the highest purity and to increase the quantum efficiency of the $InAs_{0.95}Sb_{0.05}$ active region, the As and Sb constituents of the growth-melt were added as monocrystal InAs and InSb pieces instead of the (7N's) single elements.

In the present work, by using Yb rare earth gettering of the solution during LPE growth the residual carrier concentration in the active layer was reduced up to $5*10^{15}$ cm^{-3} (T = 77 K). The cladding layers were intentionally doped with Sn up to a concentration of $5*10^{18}$ cm^{-3} and with Zn up to $1*10^{18}$ cm^{-3} for the n-and p-type layers, respectively. The epitaxial structures were grown onto (100) oriented p-type InAs substrates obtained from Wafer Technology Ltd. Laser diodes were fabricated from the epitaxial wafers using standard procedures by employing conventional photolithography and wet chemical etching to produce mesas 90 μm. Ohmic contacts were formed by thermal evaporation of Au:Zn and Au:Te alloys.

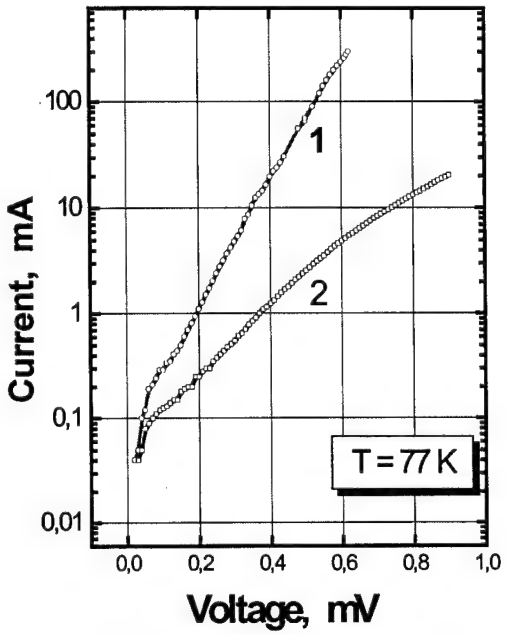

Fig.4. Current-voltage characteristic of the type I InAsSb/InAsSbP DH laser.

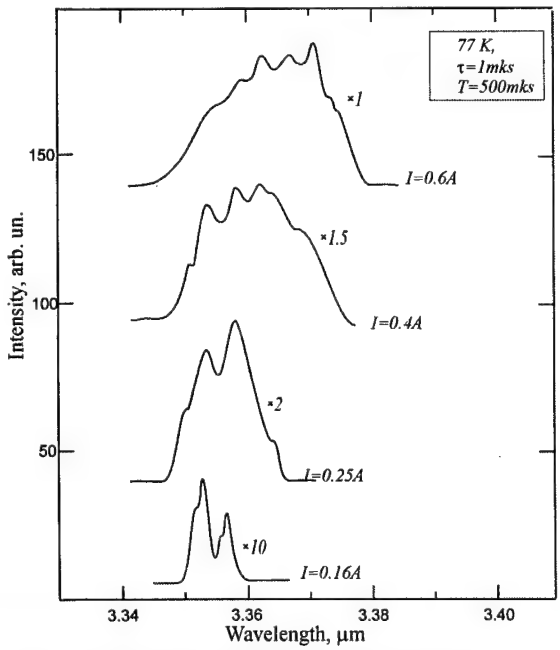

Fig.3. Multi-mode spectra of coherent emission vs the drive current in pulsed mode for type I broad-area (d=90μm) InAsSb/InAsSbP laser

Current–voltage characteristics were measured using an automatic system, based on an IC LM759 op-amp which features high-output-current capability, designed to operate from a single or dual power supply with an input common mode range that includes the negative supply. The data was read by a GPIB interface card that was connected to a voltage calibrator, voltmeter and

ammeter, and was plotted automatically. Typical I-V characteristics at 77K of type I InAsSb/InAsSbP laser shown in Fig.4, where curves 1 and 2 refer to forward and reverse applied bias, respectively. Value of differential resistance not exceed R=0.47 Ohm.

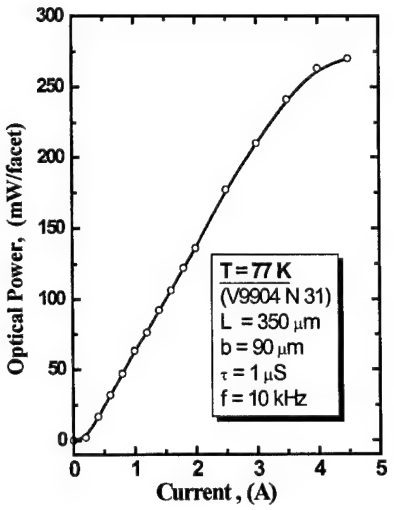

Fig.6. Power-current characteristics of broad-area InAsSb/InAsSbP laser

The electroluminescence emission spectra from the LDs and light–current characteristics were typically measured at 77 K using 1 μs current pulses of up to 10A and a frequency of 2 kHz. After passing through the cryostat windows the radiation was collected using CaF2 lenses and focused into a one-meter monochromator. The electroluminescence was detected using a cooled (77 K) InSb photodiode detector and Stanford Research (SR850) digital phase-sensitive detectorThe resulting epitaxial structures were processed using conventional photolithography and were mesa-etched into 300μm diameter surface light emitting diodes. Ohmic contacts were formed by thermal evaporation of Au:Zn + Au on the p- and Au:Te + Au on the n-side of the diode, respectively. Two kinds of lasers with narrow stripe (d=10 μm) and broad area one (d=90 μm) were fabricated.

Spontaneous and coherent emission spectra were measured in the range 77-180K in pulse mode (τ=1 μs, f=200 Hz) as well as optical power current characteristics. Spectra of coherent emission in pulsed mode at different drive current is shown in Fig.5 (T=77K). Wavelength of emission changes from λ=3.35μm up to λ=3.37μm with the current increasing. Temperature dependence of threshold current with T_0=25K was obtained for this structure in the range 77-200K. InAsSb/InAsSbP DH laser with broad area stripe (d=90μm) demonstrates multi-mode generation in pulsed mode regime. Maximum output power P=250mW was achieved in this laser structure.

6.2. InGaAsSb/InAsSbP DH lasers grown by LPE on n-InAs (111)A substrate

Double heterostructures including a wide-gap cladding layers n-$InAs_{1-x-y}Sb_xP_y$ and p(Zn)-$InAs_{1-x-y}Sb_xP_y$ ($0.05\le x\le 0.09$, $0.09\le y\le 0.18$) and an active layer n-$In_{1-v}Ga_vAs_{1-w}Sb_w$ ($v\le 0.07$, $w\le 0.07$) were grown by LPE on undoped n-InAs (111)A substrate with carrier concentration $n=1\text{-}2\cdot 10^{16}cm^{-3}$. The thickness of the wide-gap layers ranges from 4 to 6 μm,

and of the active layer from 1 to 4 μm. The mesa-stripe laser structures were fabricated by wet etching. Stripe widths were 10 and 20 μm. Cavity lengths were from 300 up to 700 μm.

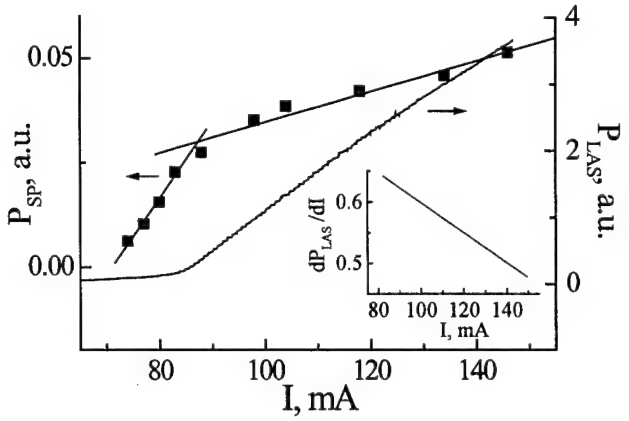

Fig.7. Current dependence of the total intensity of spontaneous P_{SP} and laser P_{LAS} emission (T=77 K, L=300 μm); the inset plots the differential quantum efficiency as a function of the current.

Spontaneous and coherent emission spectra were studied as well as differential quantum efficiency in dependence on cavity length. Fig.7 represents current dependence of the total intensity of spontaneous P_{sp} and coherent P_{las} emission (T=77K, L=300μm). Differential quantum efficiency is shown in the insert.

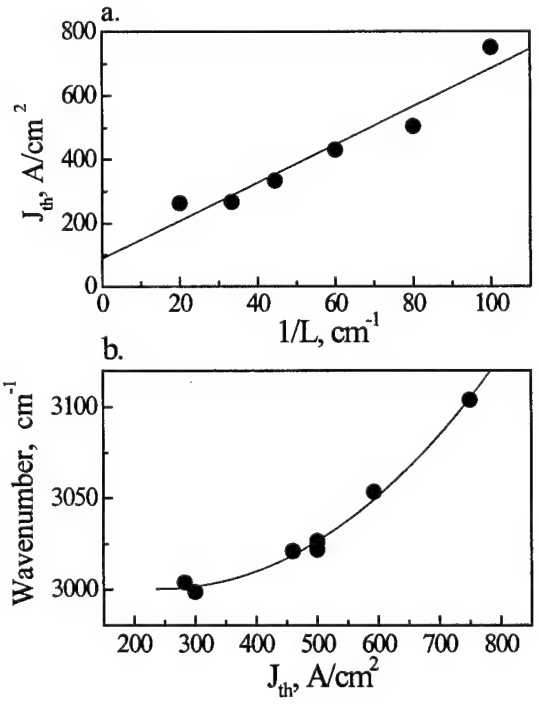

Fig.8. Threshold current density versus inverse cavity length (a); spectral-threshold characteristic (b) (T=77 K).

Threshold current density versus cavity length were also studied (Fig.8). With decreasing cavity length, the increase of the threshold current density as a result of the increase of the output losses leads to increase of the intraband absorption and to a steeper dependence of $J_{th}(1/L)$ than in the absence of intraband absorption.

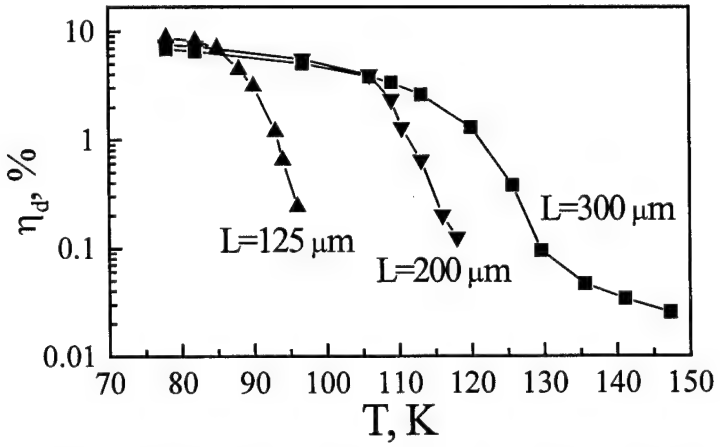

Fig.9. Temperature dependence of the differential quantum efficiency of lasers with cavity lengths L=125, 200 and 300 μm.

Temperature dependence of quantum efficiency for similar laser structures with various cavity length is represented in Fig.9. As one can see temperature dependence becomes more sloping for the longer cavity.

The magnitude of the intrinsic losses α_0 was determined from the dependence of the threshold current density J_{th} on the inverse cavity length 1/L:

$$J_{th} = \frac{J_o d}{\eta} + \frac{d}{\eta \Gamma \beta}\left(\alpha_i + \frac{1}{L}\ln\frac{1}{R}\right),$$

were J_o is the nominal current density at the threshold of inversion, d is the thickness of the active region, β is differential gain. We obtained α_0~5 cm^{-1}. The low walue of α_0 is an evidance of the structural perfection of the quaternary solid solutions InGaAsSb lattice-matched to InAs(111)A substrate.

Optical power can be evaluated as P=25mW in cw mode for narrow-stripe (d=10μm) InGaAsSb/InAsSbP lasers grown on n-InAs (111)A substrates.

6.2.1. High-power broad-area (200 μm) InGaAsSb(Gd)InAsSbP DH laser structures

There has been an increased interest in mid-infrared (3-6 μm) LEDs and diode lasers

for environmental monitoring. Such sources are especially attractive for fibre optic applications and spectrometers because of small size and high efficiency in the spectral range where most of industrial gases have fundamental absorption bands. Many researchers are now concentrating their efforts on studying the capabilities of III-V materials since these posses high thermal conductivity and metallurgical stability compared with II-VI and IV-VI systems.

The above research includes quantum well, quantum cascade and double heterostructure lasers. Broad contact (250×1500 μm) InAsSb/InAlAsSb[22] strained quantum well lasers (λ=3.4 μm) exhibited low threshold (j_{th}=44 A/см^2) and output power up to 215 mW per facet in CW mode at 77K. 100x2000μm mesa stripe lasers with InAs/GaInSb/InAs/AlGaAsSb quantum wells emitted 143 mW (I=4 A, CW, 78 K) at λ=3.03 μm[23]. Mirror-like facet and untireflection facet (R=25 %) have been employed for laser cavity. The output was limited by Joule heating of the active layer which manifested in sub-linear power-current dependence and saturation at I~4 A. The shortest reported wavelength of QCL is λ=3.49 μm achieved in InGaAs/AlInAs system[24]. 10-14 μm wide lasers can operate at pulse mode with j_{th}=2 кА/см^2 (50 ns, 4.5 кHz, 77 K) up to T=280 K. However, CW mode was accompanied by strong laser degradation and CW operation was observed at T<50 K only: I_{th}=1.2 A, 20 мВт (I=1.7 A). It is worth to mention that DH lasers are still superior to all other constructions in terms of the output power. Rubaltowski[3] reported 0.85W (I=7A, τ=4-7μs, f=200Hz) for the output of 100×700 μm InAsSbP/InAsSb/InAs DH lasers (λ=3.2 μm, T=77 K). He also reported linear light-current dependence and the increase of output power up to 2.85W for the 3 laser array (3x(100x700)μm)) at I=30A.

Most of the above laser structures have been fabricated on (100) oriented substrate. However, it is well known that the growth rate of the epitaxial layers is much higher on the (100) face than on the (111) face[25]. High quality heterojunctions with good surface morphology are thus the expected features of (111) grown layers. Moreover, impurity segregation is also orientation dependent[26] and thus one can expect that doping as well as lasing parameters of InAs based devices will depend on substrate orientation.

The aim of the work was to investigate high power InGaAsSb(Gd)/InAsSbP DH lasers emitting at λ≅3.3 μm grown on (111) InAs substrates. Epiwafers were grown by LPE method from Gd doped melts (X^l_{Gd}=0.004÷0.005 at.%) as described elsewhere[27], providing redution of residual impurity concentration and the increase of mobility in n-$In_{1-v}Ga_vAs_{1-w}Sb_w$ (n=5×10^{15}см$^{-3}$)[28]. The «purification» effect was accompanied by the increase of

photoluminescence intensity increase similar to the described in. Epilayers were processed into structures with broad contacts w=200 μm with cavity length ranging from 100 to 700 μm. Power measurements were performed in a $\pm 11^0$ angle by thermocouple detector MKS-18A with integration of spatial radiation distribution.

Fig.10 presents threshold currents and reciprocal differential efficiency vs reciprocal cavity length. The lowest threshold (j_{th}=130 A/cm^2 ,I_{th}=164 mA, L=630 μm) is two times higher that previously reported values, which can reflect worse optical confinement in our lasers (Γ≅0.4). The extrapolation of the dependence in Fig.10 through the use of standard approximation:

$$\eta_d^{-1} = \eta_i^{-1}\left(1+\alpha_i / \alpha_R\right)$$

η_d – is the differential quantum efficiency, η_i – is the internal quantum yield , α_i – are the internal losses, $\alpha_R = \ln(R^{-1})/L$ - are reflection losses (R=0.31) enable us to determine the following values: η_i=43 % и $\alpha_i \cong 10$ см$^{-1}$. The obtained values are close to the best parameters of lasers emitting at 3 μm reported early.

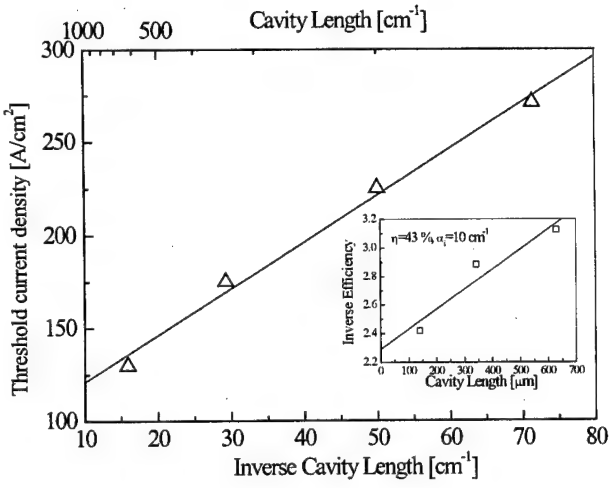

Fig.10 The dependence of the threshold current density vs the cavity length

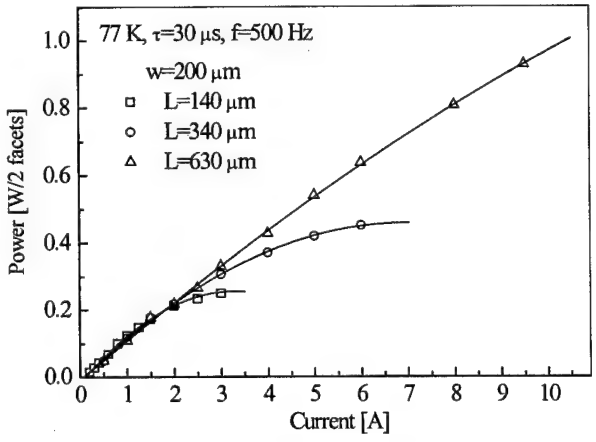

Fig.11. The dependence of the output power vs drive current

Fig.11 presents total power – current dependence in pulsed mode. As seen from Fig.11 output as high as 0.93 W is achieved at I=9.5 A. Short cavity laser power saturate because of Joule heating: 23W are to be dissipated in laser with serial resistance (R_S) of 0.23 Ω. Far field pattern is a Gaussian with a FWHM of 35^0-40^0.

In conclusion we have shown that LPE grown InGaAsSb(Gd)/InAsSbP DH lasers emits 1W pulse power at λ=3.3 μm with practically linear power-current dependence for a 200x600μm stripe. We are optimistic that future research steps (the

increase of stripe width, laser construction optimisation, matrix assembling) will further increase the output power of InGaAsSb(Gd)/InAsSbP DH lasers.

6.3. Type II asymmetric GaInAsSb/InGaAsSb/InAsSbP laser heterostructure

Recently a novel tunnel-injection laser based on type II broken-gap GaInAsSb/InAs heterojunction was proposed by us and realized[29,30]. This laser structure showed a good performance properties such as high operating temperature and low threshold current. Here, we used it as a base structure to create the laser with improved output power characteristics.

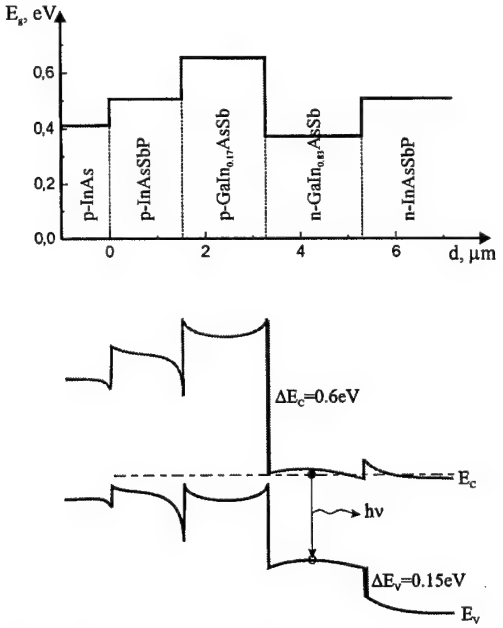

Fig.12. Schematic energy band diagram of type II asymmetric double heterostructure laser based on InAsSbP/GaInAsSb/InGaAsSb

Type II GaInAsSb/InGaAsSb/ InAsSbP laser structures with asymmetric band offset confinements were grown by LPE lattice-matched to p^+-InAs (100) substrates. Schematic laser structure and energy band diagram are presented in Fig.8. The undoped narrow-gap n-$InGa_{0.17}AsSb_{0.20}$ active layer (E_g=0.380eV at 77K) was sandwiched between doped wide-gap p-$GaIn_{0.17}As_{0.22}Sb$ (E_g=0.635eV at 77K) and n-$InAsSb_{0.12}P_{0.26}$ (E_g=0.517eV at 77K) cladding layers. This asymmetric heterostructure allows to form the separate potential barriers at the heteroboundaries of the active region: for electrons at the InGaAsSb/GaInAsSb heterointerface (ΔE_C=0.6eV) and for holes at the InGaAsSb/InAsSbP one (ΔE_V=0.15eV). The thickness of InGaAsSb layer was 0.8μm and the thickness of cladding layers were found as 2μm. The carrier concentration of active layer was $n=2*10^{16}cm^{-3}$ and doping of the wide-gap layers was about of $p=5*10^{16}cm^{-3}$ for GaInAsSb and $n=1*10^{17}cm^{-3}$ for InAsSbP.

Mesa-stripe laser structures were fabricated by standard photolithography with broad area (d=110μm) stripe and cavity length L=350-750μm. Luminescent properties of the laser structures were investigated under steady-state conditions and pulsed mode with pulse duration as τ=300ns and repetition rate f=10kHz.

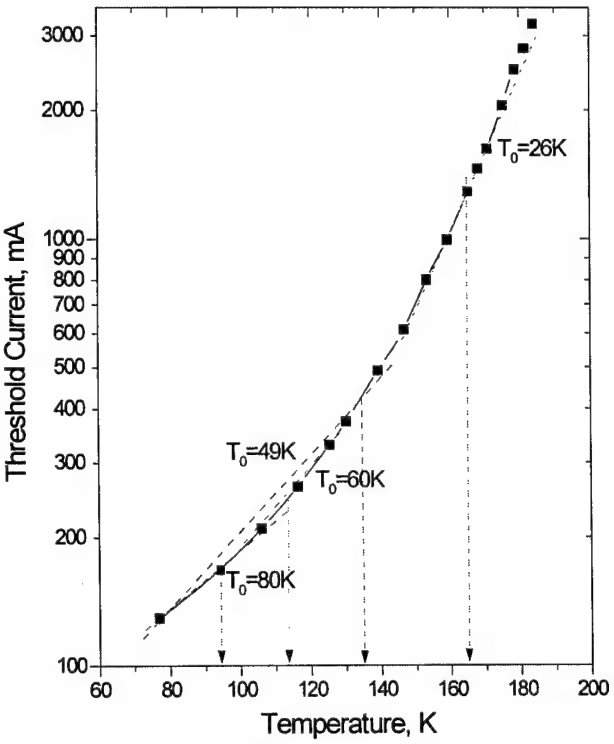

Fig.9. Temperature dependence of threshold current for type II asymmetric band-offset heterostructure based on GaInAsSb/InGaAsSb/InAsSbP

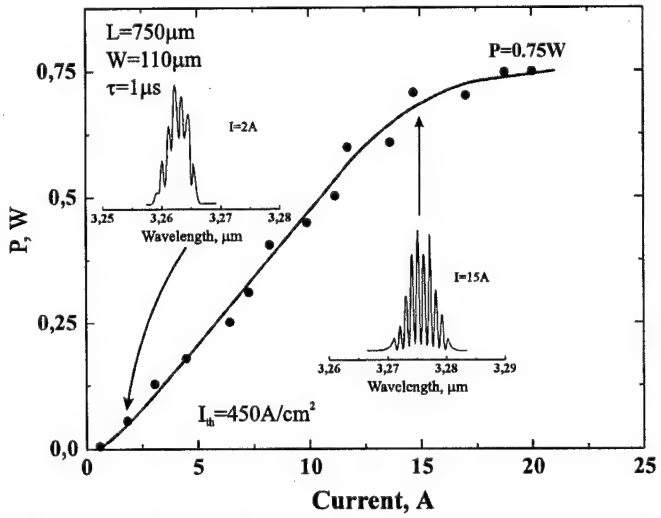

Fig.10. Optical power versus drive current for type II GaInAsSb/InGaAsSb/InAsSbP laser

In these structures we observed intense spontaneous and coherent emission in 3-4μm spectral range at 77K. Single-mode lasing for laser-stripe structure with d=100μm and L=750μm was observed at wavelength λ=3.26μm and a threshold current density j_{th}=450mA/cm^2 at 77K was obtained.

It was found that the threshold current depended only weakly on temperature at the 77-135K range, whereas the value of the characteristics temperature (T_0) decreased from 80K to 60K, so the high average T_0 value of 49K was observed. Fig.13 demonstrates temperature dependence of the threshold current for type II GaInAsSb/InGaAsSb/InAsSbP laser.

Output power up to 0.7W under pulse mode and 20mW in cw mode at 80K with multi-mode lasing was achieved for the broad-area laser with (Fig.14).

6.4 Type II AlGaAsSb/InGaAsSb double heterostructure with high asymmetric band offsets.

Recently, type II AlGaAsSb/InGaAsSb double heterostructure with high asymmetric band offset confinement was proposed by us as a way to suppress a leakage current in mid-IR diode lasers[31].

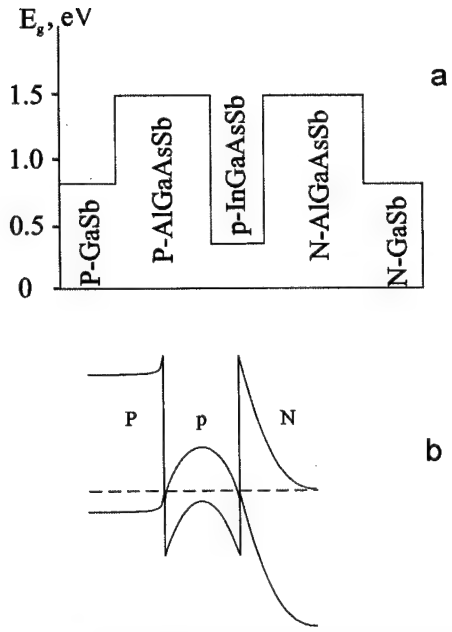

Fig.15. Schematic layer profile (a) and band energy diagram of a type II P-AlGaAsSb/p-InGaAsSb/N-AlGaAsSb heterostructure in thermodynamic equilibrium (b).

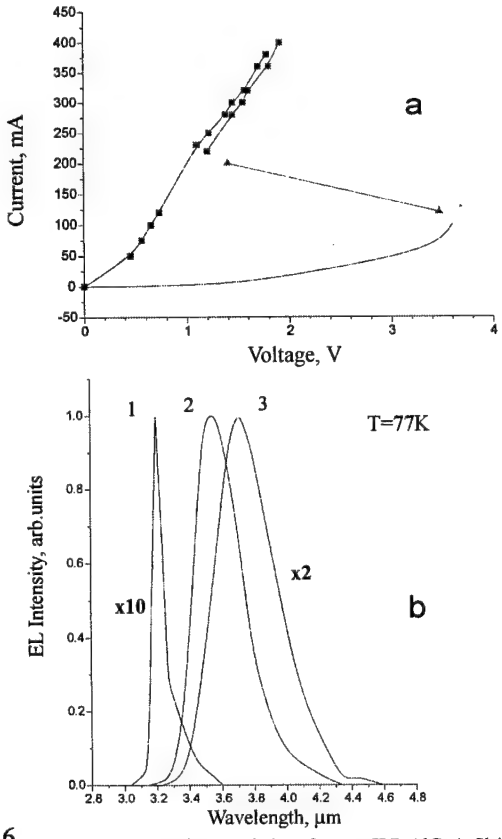

Fig.16 Current-voltage characteristics of a type II P-AlGaAsSb/p-InGaAsSb/N-AlGaAsSb double heterostructure under forward bias (a) and EL spectra for various bias voltages (1- 1.1V, 2- 1.4V, 3- 1.8V) at 77K (b).

The $Al_xGaAsSb/In_yGaAsSb/Al_xGaAsSb$ laser structures with narrow-gap active layer (y=0.94, Eg=0.326 eV) and wide-gap cladding layers with high Al content (x=0.64, Eg=1.474 eV) were grown by LPE lattice-matched to GaSb (100) substrates. The thickness of active region was about 1μm and thickness of confined layers were 2 μm. The narrow-gap active layer was doped by Zn to $10^{17}cm^{-3}$. The carrier concentration of P- and N-type wide-gap confined layers were $2*10^{17}$ cm^{-3}.

The $Al_{0.64}GaAsSb/In_{0.94}GaAsSb$ heterostructure was of type II (near broken-gap) with strong asymmetric band offsets: ΔE_C=1.35eV and ΔE_V=0.2eV (Fig.15). Mesa-stripe laser structures with cavity length 350 μm and stripe width 11 μm were made by standard photolithography. EL spectra were investigated under quasi steady-state conditions with drive current pulse duration of 2 ms and off-duty factor equal to 2.

A strong bistability of the current versus applied bias was observed in the forward branch of the current-voltage characteristics. The I-V characteristics has S-shape with a negative differential resistance (NDR) interval and turn-on voltage U_{on}=3.6V (Fig.16a).

Intense electroluminescence (EL) was observed at the spectral range 3-4μm at 77K. Emission spectrum at low drive current has a single asymmetric band with photon energy at maximum hν=370 meV (λ=3.34 μm) and FWHM about of 7-10 meV at T=77K. Blue shift of the emission maximum up to 50 meV relative to the energy gap of the active layer (Eg=326 meV) of the laser structure was observed. With drive current increasing the maximum of the emission band moves to lower photon energy values. Under high external bias it jumps to hν=326meV (λ=3.8 μm) that corresponds to the emission wavelength of bulk radiative recombination in the active region.

We assume that the intense EL in P-AlGaAsSb/p-InGaAsSb/N-AlGaAsSb double heterostructure represents a superposition of two radiative recombination processes: interface indirect (tunneling-assisted) optical recombination of electrons and holes localized at the P-AlGaAsSb/p-InGaAsSb heterointerface and bulk recombination due to interband radiative transitions in the narrow-gap p-InGaAsSb layer[32]. Such heterostructures with strong asymmetric band offset confinement can be used to design high-efficient current-controlled mid-IR lasers and light sources.

7. Theoretical calculation of intravalence band absorption (IVA) and gain in InAs-based lasers.

The mechanism of intraband absorption of radiation with hole transition into the spin-orbit split-off band, or so-called intravalence-band absorption (IVA), is subjected to microscopic analysis.

The maximum working temperature of long-wavelength lasers is known to depend on the rate factor of nonradiative channels for the recombination of nonequilibrium carriers, but it also depends on the intraband radiation absorption coefficient. An analysis has shown that the intraband absorption mechanism depends significantly on the actual band structure of the semiconductor. A unique attribute of the band structure of InAs and solid solutions of similar composition is the fact that the width of the band gap E_g is close to the spin-orbit splitting Δ. Consequently, radiation generated in a laser with $\hbar\omega \sim E_g$ would be highly prone to strong absorption by holes in the valence band, which are excited into the spin-orbit split-off band in this case.

We propose to show that intravalence-band absorption (IVA) is one cause of the low quantum efficiency of lasers made from InAs and solid solutions of similar composition. We look at the recombination processes in $InAs_{1-x}Sb_x$ and calculate the IVA coefficients

associated with transitions of heavy and light holes into the split-off band. The IVA coefficients and the optical gain are calculated in the 4-band Kane model[9], which is fully applicable to InAsSb, where the wave vectors of all particles involved in absorption are small by virtue of the closeness of E_g to Δ.

The absorption coefficient α end the optical gain g are expressed in terms of the imaginary part of the dielectric permittivity ε'':

$$\alpha = -g = \frac{\omega}{c\sqrt{\varepsilon_\infty}}\varepsilon''(\omega) \qquad (1)$$

where ε_∞ is the rf dielectric permittivity, and c is the speed of light,

$$\varepsilon''(\omega) = \lim_{q\to 0}\frac{4\pi^2 e^2}{q^2}\int\frac{d^3k}{(2\pi)^3}\left|M(\mathbf{k},\mathbf{q})\right|^2(f_1 - f_2)\times\delta(E_1 - E_2 - \eta\omega), \quad (2)$$

Where **q** is the photon wave vector, **k** is the particle wave vector, e is the electron charge, E_1, E_2, f_1, and f_2 are the energies and Fermi distribution functions of the charge carriers, and M(**k**,**q**) is the matrix element of transition between the Bloch wave functions of the initial and final states.

Integrating Eq (2) over the angles and over **k** with allowance for the delta function, we obtain equations for the IVA coefficients for transitions into the split-of band both from the heavy-hole band α_n^{SO} and from the light-hole band α_l^{SO}:

$$\alpha_n^{SO} = A\frac{M_{SO,n}^{5/2}(\eta\omega - \Delta)^{3/2}}{1+\exp\left[\dfrac{M_{SO,h}}{m_h}\dfrac{\omega-\Delta}{T} - \dfrac{\zeta_h}{T}\right]} \qquad (3)$$

$$\alpha_l^{SO} = A\frac{17E_g^2 + 20E_g\Delta + 6\Delta^2}{3E_g^2}\frac{M_{SO,l}^{5/2}(\Delta - \eta\omega^{3/2})}{1+\exp\left[\dfrac{M_{SO,l}}{m_l}\dfrac{\Delta-\eta\omega}{T} - \dfrac{\zeta_h}{T}\right]} \qquad (4)$$

where

$$A = \frac{2\sqrt{2}e^2}{\sqrt{\quad}}\frac{E_g}{\Delta^2} \qquad M_{SO,i} = \frac{m_{SO}m_i}{\pm(m - m_i)}$$

m_{SO} - is the effective mass of a hole in the split-off band.

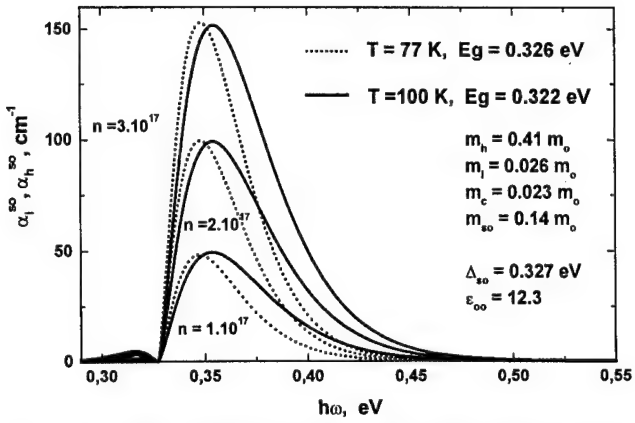

Fig. 17 3. Frequency dependence of the intravalence band absoption for $InAs_{0.9}Sb_{0.1}$ laser structure with participation of heavy (α_h^{so}) and light (α_l^{so}) holes at 77K (1-3) and 100K (1'-3')

Here I=h or l, and the plus sign does with the subscript h.

It is evident from a comparison of α_n^{SO} and α_l^{SO} that the absorption of light by heavy holes is tens of times stronger than absorption by light holes, owing to the high density of states for heavy holes. This contrast is illustrated in Fig.17 which shows the frequency dependence of the IVA coefficient in $InAs_{0.9}Sb_{0.1}$ at the temperatures of 77 K and 100 K. The frequency dependence of α_n^{SO} is also shown in Fig.18 (curves 1'-3').

Frequency curves of the gains and IVA coefficient in InAsSb at temperatures of 77 K and 100 K are shown in Fig.18 It is evident from the figure that as the temperature increases, the coefficient g decreases as usual, and the position of the maximum shifts into the long - wavelength range as a result of the temperature dependence of E_g. It should be noted that as the carrier concentration increases, g increases as well, and the maximum of the curve shifts toward shorter wavelengths . It is evident from Fig.18 that max (g) is several times the value of max α_n^{SO} at 77 K. Moreover, the maxima shift far along the frequency scale, and IVA is small in the vicinity of max (g). At 100 K the values of max (g) decrease, and the positions of the maxima tall within a

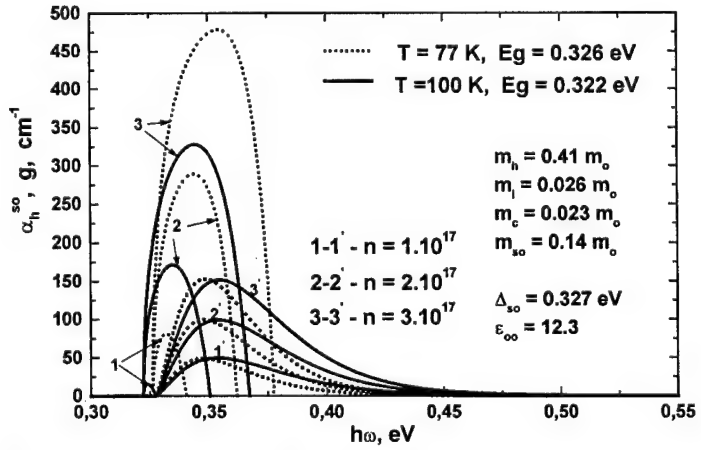

Fig. 18 Frequency curves of the gain (1-3) and IVA coefficient (1'-3') for $InAs_{0.9}Sb_{0.1}$ laser structure

common frequently interval. Consequently, IVA is already appreciable at the frequency of max (g).

It is therefore evident from Fig.18 that the coefficient α_n^{SO} becomes comparable with g in a certain range of frequencies and charge densities at given temperatures.

Semiconductors with $E_g<\Delta$ must be used to suppress the mechanism of strong absorption by HH. This condition can be achieved either by varying the temperature or by using solid solutions of the appropriate composition. For example, in InAs E_g becomes smaller than Δ at T>155 K. In $InAs_{1-x}Sb_x$ the inequality $E_g>\Delta$ holds at x<0.1 and T≈77 K. One final note of importance: in semiconductors with $E_g< \Delta$ not only the IVA is suppressed, bur Auger recombination involving the SO subband (CHHS process) also diminishes. Therefore the heating caused by Auger recombination will also be decreased.

8. MBE growing of multiple quantum wells and superlattice for mid-IR laser structures

Fabrication of high efficiency laser heterostructures, and especially those based on (Al)GaSb/InAs system, needs an optimization of all the constituent elements including superlattices (SL), cladding layers, active quantum well (QW) layers etc[18,19]. A quality of each of these elements, revealed by their structural, electrical and optical properties, has a dramatic influence on the integral characteristics of the whole laser structure. In particular, formation of the type-II InAs/GaSb QW interfaces with a certain interface bond (InSb-like or GaAs-like) gains the major importance, since atoms of both cation and anion sublattices are changed simultaneously[19]. Particularly the InSb-like interfaces are known as more preferable to provide good luminescence characteristics. Obviously, it is necessary to have a high reproducibility of thicknesses and compositions of different layers.

During the current stage of the project we performed a development of molecular beam epitaxial (MBE) technique for a fabrication of different model structures involving the key elements of a developed laser structure and allowing us to study them separately by different techniques. This approach seems to be reasonable, because the information obtained from the whole structure on its different regions is quite limited to be interpreted adequately.

Further we present the results of the studies of the following model structures performed for the first half of the project duration:

1. GaAsSb/InAs short period SLs;
2. AlSb/InAs/GaSb two-dimensional (2D) electron gas QW structures;
3. AlGaSb/GaSb multiple QW (MQW) structures and structures with double QWs;
4. InAs/GaSb MQW structures.

All the structures were grown by MBE in a Riber 32 system equipped with elemental group III and group V sources. As for the latter, we have used a standard evaporation cell producing As_4 molecules and two antimony sources, a conventional cell or a cracking cell, providing Sb_4 or Sb_2 molecules, respectively. Most of the results presented here were obtained using Sb_2. Growth temperatures were monitored using an IRCON infrared pyrometer which was calibrated before each growth run, using the substrate surface oxide desorption temperatures (GaAs - 580°C, GaSb - 560°C), and during the process using specific temperatures of surface reconstruction change (e.g. 2×4 ↔ 1×3 at about 520°C for GaAs). The surface reconstruction at different stages of the growth, in particular its transition at the type-II heterointerface, was monitored with reflection high-energy electron diffraction (RHEED).

8.1. GaAsSb/InAs short period superlattices

Strained short-period GaAsSb/InAs SLs with average lattice parameter nearly lattice-matched to InAs substrate were grown at temperature T=480°C. The SLs containing 40 periods of GaAsSb and InAs layers both of 2.5 nm in thicknesses, were embedded between two 0.5μm InAs epilayers. The crystalline perfection of the structures has been studied by a high-resolution X-ray diffraction (HRXRD), using Ge double-crystal diffractometer adjusted for (004) reflection of Cu$K_{\alpha 1}$ radiation (Fig.19).

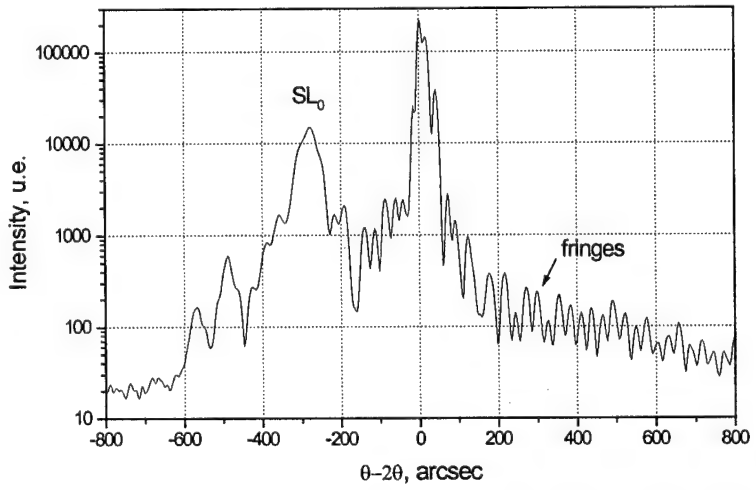

Fig.19 Double-crystal rocking curve of $GaAs_{0.05}Sb_{0.95}$/InAs SL around the (004) InAs reflection.

shows double-crystal rocking curve in a vicinity of (004) InAs reflection for the $GaAs_{0.05}Sb_{0.95}$/InAs SL. A sharp peak from InAs substrate and a well pronounced oscillating

structure showing flatness of the whole structure surface can be easily observed. Presence of the additional periodicity in the structures is proved by distinct superstructural reflections. Their angle positions indicate that the parameters of the SL are close to those expected from growth conditions. The multiple pronounced interference fringes related to both a 500 nm-InAs top layer and the SL as a whole evidence that the SL is quite perfect and has very flat interfaces. Moreover, it indicates good reproducibility of quantum layer thicknesses and high crystalline. The assumption of pseudomorphic growth (verified by asymmetric HRXRD reflections, as well as by ω-rocking curves) yields a SL-substrate mismatch of about $2 \cdot 10^{-3}$. It is small enough to grow rather long SL without stress relaxation.

These short-period SLs are planned to be used in laser structures for the following purposes:

- as part of a waveguide layer, which prevents the segregation of impurities and decreases the dislocation density in active layers of a laser as well as results in the more flat growth front;
- as a material of QW with desired effective energy gap band offsets;
- as cladding layers instead of alloy ones.

8.2. AlSb/InAs/GaSb 2D electron gas QW structures

As mentioned above, one of the important problems in GaSb/InAs system grown by MBE is a formation proper interfaces with regular atom ordering, planarity and certain interface bonds. To optimize MBE growth conditions for obtaining perfect interfaces one can use photoluminescence measurements of optical structures. But we chose more simple and fast way. We proposed to use Hall measurements carried out for AlSb/InAs/GaSb two-dimensional electron gas QW structures. This technique are known to be an effective express method to examine the quality of interfaces due to a high sensitivity of Hall mobility to different interface unhomogeneities and defects. We have grown by MBE a set of AlSb/InAs/GaSb two-dimensional (2D) QW structures at T=500°C using the Sb cracking cell as antimony source to study the effect of growth parameters and structure geometry on InAs/(AlGa)Sb interface formation. The cracking cell in comparison with a standard cell permitted one to improve quality of materials and interfaces due to using Sb or Sb_2 fluxes instead of Sb_4 flux. The internal geometry of the structures is shown in Fig.20. The AlSb barriers placed at the InAs/GaSb interfaces had different widths ranging between 0.6-100 nm. In some structures a 5 nm-InAs cap layer was used additionally to the GaSb one. All the

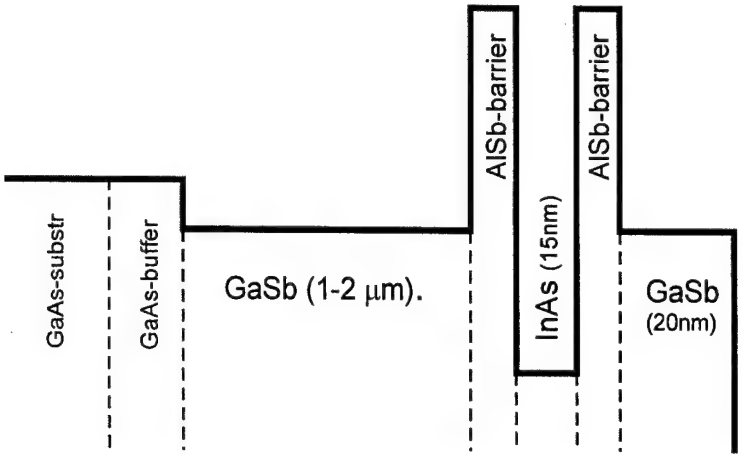

Fig.20. Schematic energy band diagram of the AlSb/InAs/GaSb two-dimensional electron gas QW structures

samples reproducibly showed extremely good transport characteristics, with low temperature 2D electron mobility exceeding 100000 cm^2/Vs at T=77K. The best sample with 3nm AlSb barriers demonstrates the Hall mobility of 26500 and 230000 cm^2/Vs at T=300K and T=77K, respectively, at corresponding electron concentrations of $2.9*10^{12}$ and $1.4*10^{12}cm^{-2}$. We hope that the structural modification of the structures will allow us to improve the characteristics further.

8.3. AlGaSb/GaSb MQW structures and structures with double QWs

During our investigations it was found out that PL intensity of AlGaSb/GaSb MQWs is very sensitive to the material quality of both GaSb and AlGaSb layers as well as to the

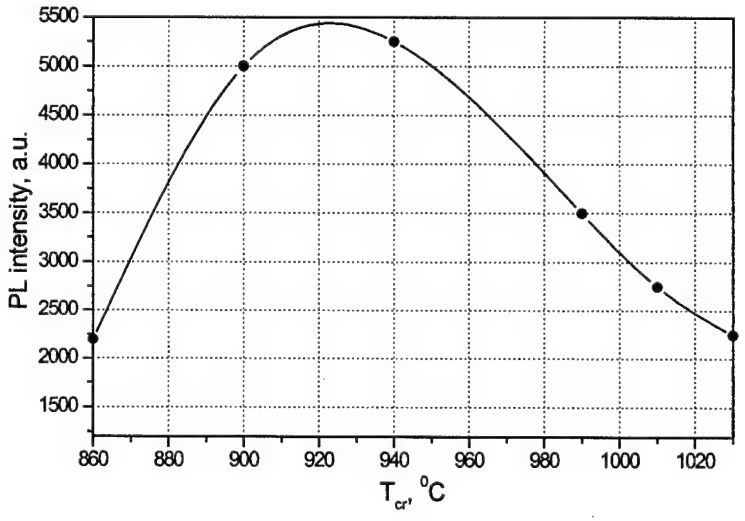

Fig.21 Photoluminescence (PL) intensity of the $Al_{0.35}Ga_{0.65}Sb$/GaSb MQW structures versus Sb cracking cell temperature (T_{cr}).

interface imperfections. Thus, these simple structures can be used for testing the materials discussed, which are used in MIR lasers as cladding layers, energy barriers for QWs etc. We have investigated the PL in AlGaSb/GaSb MQW structures grown at T=500°C using an antimony cracking cell. The PL studies were carried out with excitation by a 800 nm semiconductor laser at 77K. Ten periods of 4 nm GaSb QWs separated by 10 nm $Al_{0.35}Ga_{0.65}Sb$ barriers were placed between 50 nm $Al_{0.35}Ga_{0.65}Sb$ confinement layers. The QW thickness was chosen 4 nm, because this is the QW thickness value corresponding to the inter-valley transition $\Gamma \leftrightarrow L$ (direct to indirect optical transitions).

It is known that the cracking zone temperature of the Sb cracking cell influences on PL intensity of Sb-based structures. To optimize precisely this parameter for laser structures fabricated in our MBE system we have grown a set of the MQW structures in the same manner but at the different cracking temperatures T_{cr}. Fig.21 shows the dependence of PL intensity of the $Al_{0.35}Ga_{0.65}Sb$/GaSb MQWs versus T_{cr}. It is clearly seen that the optimal cracking temperature is about 920°C. It was also found out that the PL intensity from the sample grown at the optimal T_{cr} at least 5 times higher than that for a sample grown with a standard Sb cell.

The PL spectra for the structures grown at two cracking temperatures T_{cr}= 940°C and T_{cr}= 1030°C are shown in Fig.22. The PL spectra of the structures grown at $T_{cr} \leq$ 950°C (curve 1) contain only two narrow peaks at photon energy of 760 meV (peak A) and at about of 980 meV (peak B) that correspond to the signal from the substrate and QWs, respectively. FWHM of peak B was about 12-15 meV. PL spectra of the structures grown at T_{cr}> 950°C (curve 2) contain one more wide peak at about 880 meV (peak C). We suppose that peak C is

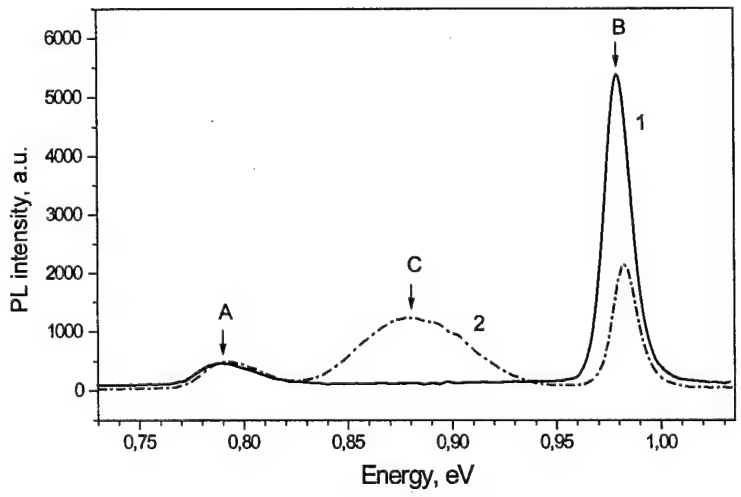

Fig.22. Photoluminescence spectra of the $Al_{0.35}Ga_{0.65}Sb$/GaSb MQW structures grown at Sb cracking cell temperature: 1) 940°C, 2) 1030°C.

due to appearance of deep levels related to impurity background rising with the increasing the cracking temperature. It should be noted that the energy value for the peak B corresponds well to the theoretically estimated response (975 meV) from a structure with 4 nm GaSb QWs, which demonstrates precise growth rate and alloy composition reproducibility.

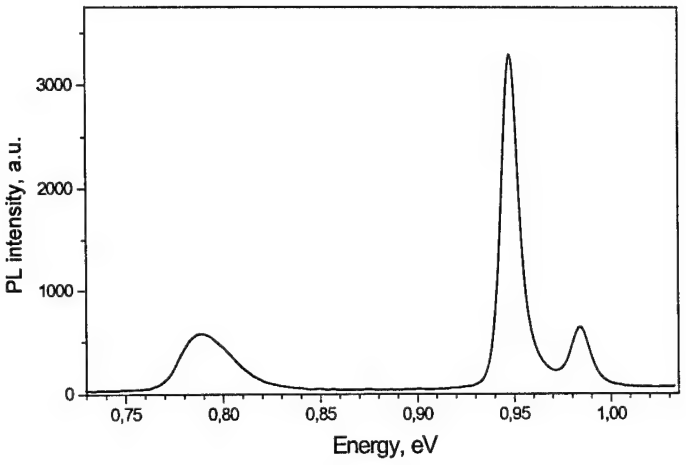

Fig.23. Photoluminescence spectrum of the $Al_{0.35}Ga_{0.65}Sb$/GaSb double QW structure.

We have also grown and investigated AlGaSb/GaSb double QW (DQW) structures containing a single QW (SQW) as a reference. Besides, the theoretical calculations of the structures were done. The width of all QWs and the barrier in DQW was 4 nm and 1.5nm, respectively. PL spectra of the structures (Fig. 23) showed two narrow peaks (FWHM is about 10 meV), besides the substrate one, with high luminescence intensities at 948 and 984 meV. The higher energy peak corresponds to the optical transition from the lowest level in SQW, while another one corresponds to the similar transition in DQW. The SQW showed a reproducible value of optical transition energy of 984 meV, close to the calculated value (975 meV). The energy difference between SQW and DQW peaks is about 36 meV and almost coincides with the calculations (35 meV). That indicates the perfection of the tunnel-thin AlGaSb barrier and GaSb wells grown by MBE as well as their high thickness accuracy.

8.4. InAs/GaSb MQWs and type II light-emitting diode structures (LEDs-2).

Five and ten periods InAs/GaSb MQW structures confined by AlSb/AlGaSb barriers have been grown by MBE and investigated by photoluminescence at 77 K. The widths of InAs QWs and GaSb layers were 1.2-1.7 nm and 30 nm, respectively. The AlSb/AlGaSb barriers were grown at a substrate temperature T= 500^0C, while InAs/GaSb MQWs were grown at about T= 420^0C. GaSb/InAs interfaces were fabricated to create preferentially InSb-like bonds. The main problem here is intermixing of group V elements at the interfaces. Since we use just conventional solid sources for As and Sb, to avoid this intermixing we used an InAs growth rate five times lower as compared to that of GaSb with the respective reduction of an As flux to keep constant the As/In flux ratio. But even in this case we believe that the

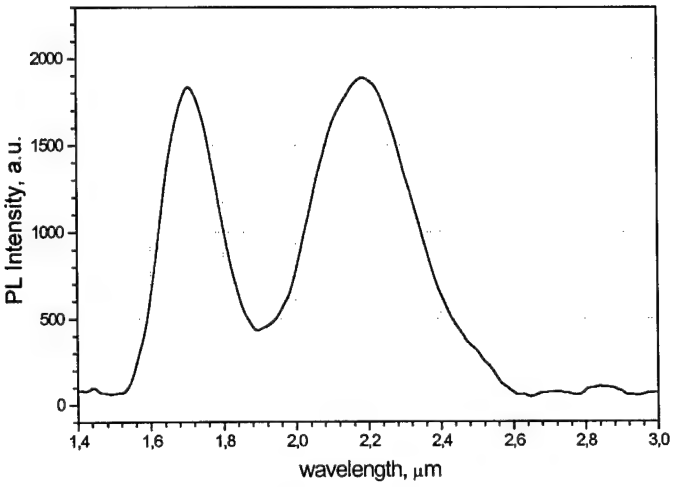

Fig.24. Photoluminescence spectrum of ten periods InAs/GaSb MQW structure with 1.7nm thick InAs QWs at 77K

intermixing still exists, which reduces significantly the PL efficiency of the InAs/GaSb QW structures. PL spectrum of the InAs/GaSb QW structure with InAs QW thickness 1.7 nm is presented in Fig.24. There are two distinct peaks in the spectrum. One of them is at 1.7 μm wavelength originating from the n-type ($n\sim10^{18}$ cm^{-3}) GaSb substrate, whereas another one is at 2.2 μm wavelength is supposed to be related to the MQW.

Recently we have obtained the multi-quantum well structures based on type II broken-gap InAs/GaSb superlattice and investigated their electroluminescent properties. The EL spectra at T=77K consisted of three emission bands with a maximum at energies 357 meV, 377 meV and 428 meV[33].

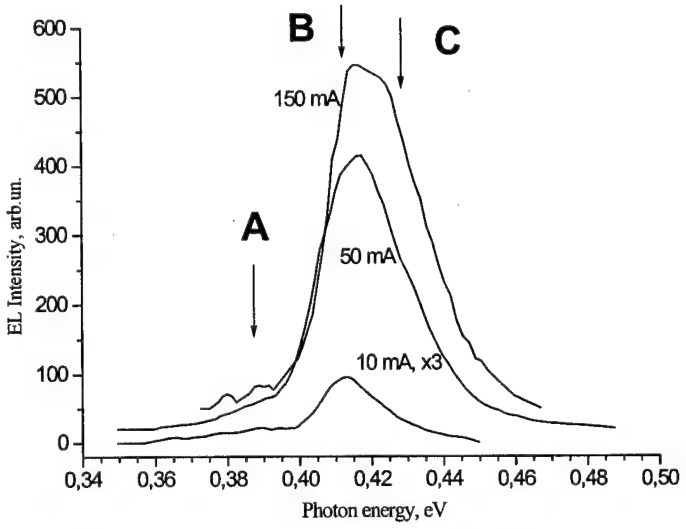

Fig.26. EL spectra of InAs/GaSb MWQ structures at T=77K

In the framework of this project the multilayer heterostructures with a $(5nm\text{-}InAs/5nm\text{-}GaSb)_3$ MQW in the active region embedded in 10 nm-AlSb barriers have been grown by MBE on a p^+-InAs (100) substrates having a hole concentration of $p\sim6\times10^{18}$ cm^{-3}. It consists of a Be-doped 0.5 μm thick p^+-InAs buffer layer followed by an active region and, finally, a Si-doped 1 μm thick n-InAs cap layer with an electron concentration $n\sim1*10^{17}$ cm^{-3}. The substrate temperature during the growth was

480°C for buffer and cap InAs layers, whereas for active region it was chosen 420°C. The growth rate was 10nm/min for GaSb and for thick InAs layers and 2nm/min for thin InAs layers. A growth interruption under antimony flux was realized at each GaSb/InAs interface in order to promote the formation of preferentially InSb-like bonds.

The samples under study were round mesa light-emitting diode structures (LEDs) with mesa diameter of 300 μm and contact diameter of 100 μm. The LEDs were fabricated by standard photolithography with deep wet chemical etching. The total size of the LED crystal was 500x500 μm^2. The chip was mounted on the TO-18 standard case. The electroluminescence (EL) measurements were made at T=77 K. The EL spectra were recorded by a MDR-4 grating monochromator with a 150 lines/mm grating by the method of syclotronous detection. The detector was a InSb photoresistor cooled by liquid nitrogen. The EL was studied in a pulsed mode with pulse duration t=2.5ms and repetition rate f=10^5Hz.

Under applied direct bias to the LED the intense EL in the spectral range 3-4 μm was observed starting from the voltage value U~0.6V. The EL spectra contain two pronounced emission bands A and B with the photon energy at the maximum $h\nu_A$=0.380 eV and $h\nu_B$=0.412 eV, respectively (Fig.26). These band have different shape: band A was close to Gaussian while the band B inhibited asymmetry with the sharp long-wavelength edge and had the short-wavelength tail which can be ascribed to the third emission band named C with the photon energy $h\nu_C$=0.425 eV. With increase in a drive current the "blue shift" of these emission bands was found (see insert in Fig.27). It should be note the band B was already dominant band in the EL spectra, while the band A demonstrated at low drive current and the band C became apparent significantly at the high current values. As seen in the Fig. 27, the curve of the EL intensity dependence on the current has three slopes. At the start stage i<10mA the emission intensity arose slowly with increasing the

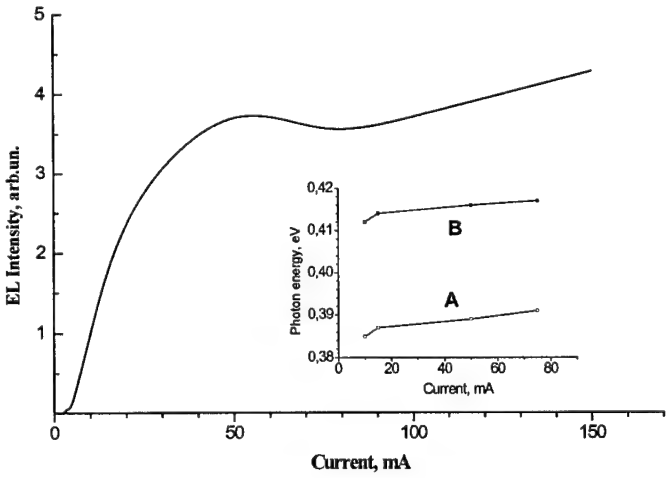

Fig.27. The current dependence of EL Intensity and emission band position (insert) for InAs/GaSb MQW structures at T=77K

drive current. The intermediate slope (10mA<i<50mA) inhibits the superluminescence mode and at the high bias the EL intensity achieved the saturation.

9. Novel asymmetric III-V/II-VI hybrid heterostructures AlAsSb/InAs/CdMgSe grown by MBE

In the framework of this project we have proposed a new theoretical model of laser structure with high (more than 3-5 kT) *asymmetric barriers* for electrons and holes at the interfaces between a narrow-gap quantum well (QW) active layer and wide-gap cladding layers, which can combine the advantages of both type I and type II lasers. In the structure the type I QW active layer is sandwiched between wide-gap N-and P- cladding materials forming a type II heteropair. This approach allows to reduce the carrier leakage from the active region of the laser structure, especially hole leakage.

There exist only three III-V compounds to design the proposed laser structures, which could provide high enough barriers for electrons and holes simultaneously: Al(Ga)Sb-InAs-InP. However, the latter is strongly lattice-mismatched to the former two, making the growth of the pseudomorphic III-V laser structure with a strong hole confinement in the InAs active layer to be a very sophisticated task for any of state-of-art technological methods (LPE, MBE, MOCVD).

A *new approach* consists in combining III-V and II-VI compounds in one Al(Ga)SbAs/InAs/Cd(Mg)Se laser heterostructure, which allows one

1) to achieve the necessary *large conduction* (ΔE_C) *and valence band* (ΔE_V) *offsets* (in excess of 1.0 eV for both cases), providing strong *carrier confinement*;
2) to keep the whole structure *pseudomorphic*, because MgCdSe alloy can be completely lattice-matched to InAs;
3) to provide excellent *optical confinement* due to the large difference in refractive index between the III-V active region (n_{InAs}=3.4) and the II-VI barrier(n_{CdSe}=2.55).

As the possible problem, one should note a difficulty in formation of high-quality CdSe/InAs interface free from the extended defects (like stacking faults and misfit dislocations) which could significantly disturb the laser structure characteristic.

Nevertheless, recently we have fabricated the first hybrid AlSbAs/InAs/Cd(Mg)Se heterostructures by MBE, consequently in two separate growth chambers. An intense photo- and electroluminescence over 3 μm have been observed in the structures both at low (77K) and room temperature. Weak temperature dependence of spontaneous emission indicates the

effective carrier confinement in the InAs layer due to high potential barriers in conduction (ΔE_C =1.28 eV) and valence (ΔE_V~1.6 eV) bands[34].

The III-V part of the structures for optical measurements was grown in a Riber 32 MBE chamber at a substrate temperature T_S=480°C on a p^+-InAs (100) substrate having a hole concentration p~6×10^{18} cm^{-3}. It consists of a 0.1 μm thick p^+-InAs:Be buffer layer followed by a 20 nm thick p-AlSbAs:Si barrier and, finally, of an undoped 0.6 μm-InAs layer (n<10^{17} cm^{-3}). AlSbAs/InAs interfaces were fabricated to create preferencially InSb bond. After growth, the wafer was covered with an As cap layer deposited during one hour at T_S<25°C. This As cover was used as a passivating layer to prevent the surface from oxidation in atmosphere, when transferring to a separate II-VI MBE chamber (home-made EP 1203) through the air. The III-V samples were stored in a nitrogen atmosphere within one week before being used for the II-VI growth.

Elemental Cd, Mg and Se molecular beam sources were employed for a Cd(Mg)Se growth [35,36]. Before the growth, the As cover was removed by annealing the sample at T_S<480°C. A RHEED system was used to control surface conditions. A (4×2)In-rich surface reconstruction was observed before II-VI growth, although different samples, having a thinner As cap evaporated at 460°C, demonstrated first a (2×4)As-stabilized surface reconstruction gradually changing to (4×2)In through the intermediate (4×4) one. The II-VI growth was initiated with a formation of In-Cd interface by a 5 s exposure of InAs surface to the Cd flux. Further, a migration enhanced epitaxy (MEE) mode was employed at T_S=200°C to grow ~10 nm of a CdSe (or CdMgSe) nucleation layer. No 3D growth stage was observed. Then T_S was raised to 280°C during growth interruption and the rest of the Cd(Mg)Se structures were grown in MBE mode at Se/Cd BEP ratio of ~3 usually demonstrating bright streaky (2×1)Se-rich RHEED pattern (VI/II=2 correspons approximately to the 1:1 flow ratio). $ZnCl_2$ was used as an n-dopant source.

Two samples (A and B) intended for luminescence measurements have the same III-V structure, but different II-VI layers grown on top. Sample A contains 830 nm of pure CdSe, followed by a 0.56 μm CdMgSe layer. Both the layers are nominally undoped. Sample B consists of 50 nm of nominally undoped CdMgSe followed by 0.3 μm of n-type CdMgSe:Cl and capped with a 10 nm-CdSe:Cl. The electron concentration of n~4×10^{17} cm^{-3} was obtained for this layer from C-V measurements. Thus, sample B is a light-emitting diode with the p-n junction placed within the InAs layer. Mg mole fraction in the layers was estimated as 12-15% from x-ray diffraction (XRD) measurements which also confirm a pseudomorphic

nature of the II-VI layers, yet the $Cd_{1-x}Mg_xSe$ composition lattice-matched to InAs is estimated as x~0.10. The cross-sectional scanning electron microscopy images of samples A and B are presented in Fig.28a and Fig.29a, respectively.

To measure photoluminescence (PL), we used single-grating monochromators and different excitation sources for different spectral regions. InGaAs cw laser diode emitting at 950 nm was used to excite PL in the III-V part of the structures, responsible for infra-red (IR) spectral region, while a 325 nm line of a cw He-Cd laser was used to excite red, yellow and green PL from Cd(Mg)Se.

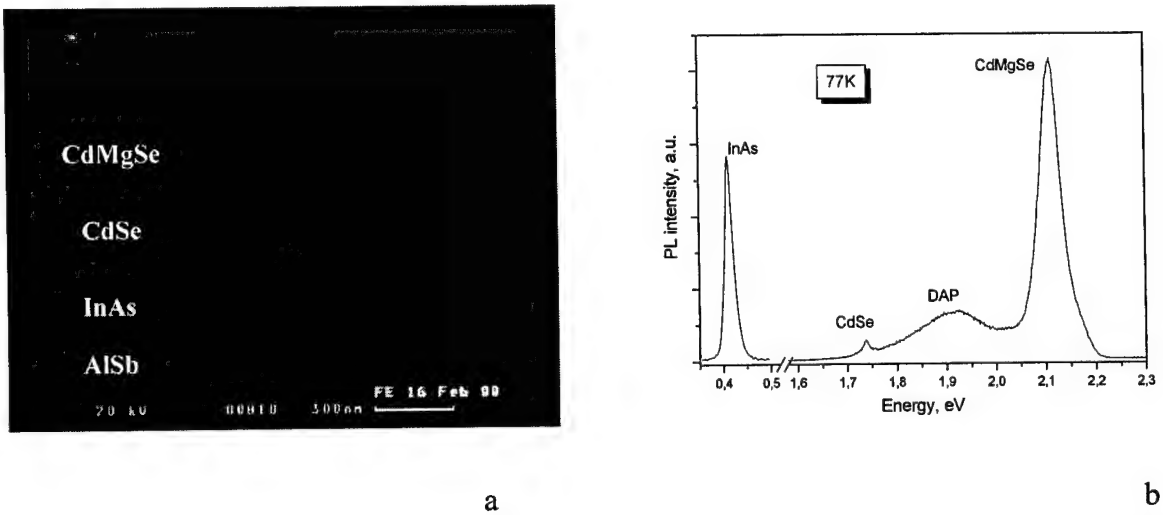

a b

Fig.28. Cross-sectional SEM image (a) and PL spectra at 77K (b) of undoped AlSb/InAs/CdSe/CdMgSe structure.

Figure 28b outlines the PL spectra measured at 77K in sample A. Three relatively narrow peaks are visible at 0.41 eV, 1.737 eV and 2.111 eV, which are attributed to the near-band-edge PL in InAs, CdSe, and CdMgSe layers, respectively. Additionally, a wider peak is seen near 1.9 eV, resulting, most probably, from a DAP recombination in CdMgSe. The InAs and CdMgSe related peaks are observed also in the spectra of sample B (see Fig.29b).

We have also studied EL of the structure. For these studies, the mesa diodes of 300 μm diameter with a 50 μm round contact were fabricated using a standard photolithography and deep wet chemical etching. EL spectra were measured using a MDR-4 grating monochromator and a lock-in amplifier. A liquid N_2-cooled InSb photodetector was used for light detection. Spontaneous EL spectra were measured both under quasi-cw conditions with pulse duration of t = 2.5 ms and filling factor of 1/2 and in a pulsed mode with pulse duration t = 1-10 μs and a repetition rate f = 10^3-10^4 Hz.

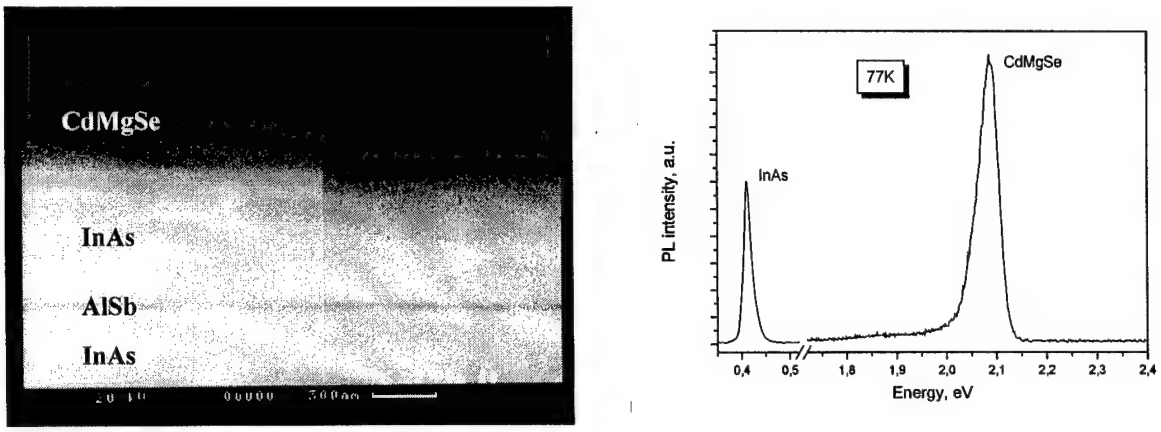

a b

Fig.29.Cross-sectional SEM image (a) and PL spectra at 77K (b) of p-InAs/p-AlSb/i-InAs/n-CdMgSe/n-CdSe p-i-n diode structure.

The intense electroluminescence has been found at both 77 and 300K as shown in Fig. 30. The EL spectrum at 77K contains a single emission band with a photon energy maximum at hν = 430 meV and linewidth FWHM = 40 meV. The emission band had a weak asymmetric shape with abrupt high-energy edge. The room temperature EL spectrum contains also the single emission band with a photon energy maximum at hν = 396 meV and FWHM = 68 meV, although the peak has a reverse asymmetry with a noticeable short-wavelength tail. The photon energy of the spontaneous EL is close to the long-wavelength PL peak maximum observed in Fig. 29.

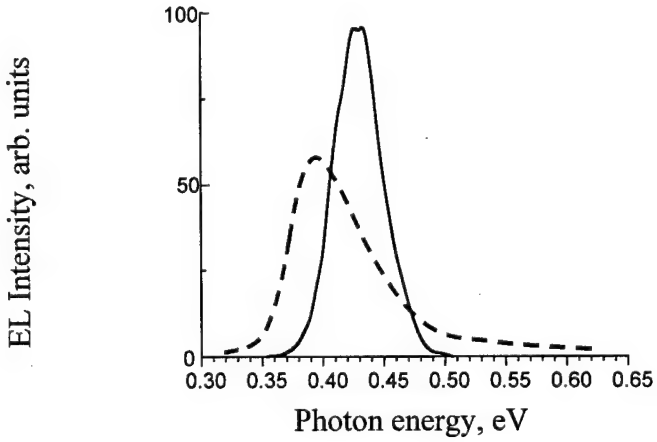

Fig. 30. EL spectra of InAs/AlAsSb/InAs/CdMgSe/CdSe laser structure at 77K (solid line) and 300K (dashed line).

The dependences of EL intensity on a drive current at cw and pulsed modes were studied also both at low and room temperatures (Fig. 31). One should note that the dependence of spontaneous emission at 77K exhibits the behavior close to a superluminescence regime.

With the temperature increasing from 77 to 300K, the maximum EL intensity decreases just by 7-10 times. This weaker temperature dependence of the spontaneous emission, as compared to that observed in conventional InAsSbP/InAs-based laser structures, evidences a rather high band offsets and better hole confinement in the hybrid structure.

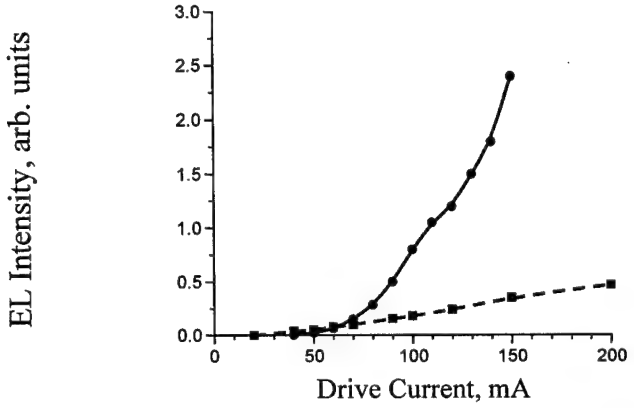

Fig. 31. EL intensity as a function of drive current at 77K (solid line) and 300K (dashed line).

To our mind, these findings together confirm high structural perfection of the formed InAs/Cd(Mg)Se heterointerface, but do not provide direct information about the respective band line-ups. Indeed, all the emission bands observed can be ascribed to the respective bulk materials, in good agreement with the strain situation in the sample and the data of XRD measurements.

To estimate the band-offset at the InAs/CdSe inerface we used the "model-solid theory" of Van de Walle[37], which suggests the type II band line-ups. InAs represents a ~60 meV potential barrier for electrons at the bottom of the CdSe conduction band, whereas the heavy hole band offset at the interface is as large as ~1.42 eV. Different situation is expected for the InAs/CdMgSe interface for the large enough content of Mg. The energies of the CdSe and CdMgSe emission bands taken from the spectrum in Fig. 28b allow estimation of the band gap difference between the two materials as about 370 meV. One can expect that at least a half of this value falls on the conduction band offset, resulting in the strong type I band alignment with the conduction band offset at least larger than 120 meV.

In conclusion, first hybrid Ga(Al)Sb/InAs/Cd(Mg)Se heterostructures have been fabricated consequently in two separate MBE chambers. The RHEED, XRD, PL and EL measurements performed allow one to conclude about high structural perfection of the InAs/CdMgSe interface in the structures. Preliminary results on electron transport

measurements along the InAs/Cd(Mg)Se interface are in good agreement with the theoretical estimation of the InAs/CdSe band line-ups giving the type II band offsets of ~60 meV and 1.42 eV for conduction and valence band, respectively. Increase in Mg content in CdMgSe should result in the strong type I band alignment at the CdSe/InAs interface.

10. Conclusion and outlook.

In the frame of this Proposal III-V mid-infrared lasers for the spectral range 3-3.6 μm of various designs were fabricated and their electroluminescence and optical power characteristics were studied.

1. Conventional type I InAsSb/InAsSb/InAsSbP lasers grown by LPE lattice-matched on InAs (100) or on InAs (111A) substrate were made with undoped active region or doped by rare earth (Gd) to improve material morphology and to reduce carrier concentration.
2. Type II heterolasers based on GaInAsSb/InGaAsSb/InAsSbP with asymmetric band offset confinement in conduction and valence bands (ΔE_c=0.60 eV, ΔE_v=0.15 eV) were grown by LPE. Weaker temperature dependence of the threshold current and the higher characteristic temperature up to T_0=47-60K (instead of T_0=25-30 for traditional DH laser structure) were obtained in the range 77-140K.
3. Theoretical model of a novel asymmetrical laser structure with large barrier heights in the conduction and valence bands was proposed to improve temperature and power characteristics of mid-IR lasers.

   New laser structure combining some positive features of the type I and type II heterostructures was considered.

   Efficient suppression of injection current in proposed asymmetrical laser structure was predicted.
4. High optical power in pulsed mode up to 1W was achieved in type I lasers InGaAsSb(Gd)/InAsSbP grown on InAs (111A) substrate with improved design and broad-area stripe (200 μm x 600 μm). Further optimization of the laser design allows reaching more optical power both in pulse and in cw-mode.
5. Multiple quantum wells InAs/GaSb, AlGaSb/InAs/GaSb and short period superlattices (GaAsSb/InAs) were grown by molecular beam epitaxy. 2D-electron gas parameters were studied in AlSb/InAs/GaSb QW structure and high mobility at the interface 100, 000 cm^2/vs at 77K was observed. MBE growing conditions were studied to fabricate MQW layers with good quality interface for mid-IR laser structure. Photo-and electroluminescence of MQWs were studied in the range 3-4 μm.
6. The most pronounced result is a proposition and relization of a new hybrid laser structure with strong asymmetric band offset confinement on the base III-V/II-VI materials. For the first time an original MBE technology was used to create p-AlAsSb/i-InAs/n-Cd(Mg)Se hybrid structure with high band-offsets (ΔE_c=1.28 eV, (ΔE_v=1.6 eV) and good optical

confinement (n=) Effective electroluminescence with weak temperature dependence was observed at 77-300K. It allows us to hope on achievement of coherent generation in these laser structures up to room temperature.

These results show that further investigation must be concentrated on band-gap designing, optimization and study of a novel hybrid II-VI/III-V heterostructure which is very promising for fabrication of high-power mid-ir lasers with improved parameters. Such laser structures can be realized with using novel MBE and MOCVD technology methods.

Reference

1. P.Werle, Appl. Phys. Lett B60, 499 (1995)
2. S.R.Kurtz, R.N.Biefield, A.A.Allerman, A.J.Howard, M.H.Crawford, M.W.Pelczynsi, Appl. Phys. Lett, 68, 1332 (1996)
3. A.Rybaltowski, Y.Xiao, D.Wu, B.Lane, H.Yi, H.Feng, Y.Diaz and M.Razegi, Appl Phys Lett 71, 2430 (1997)
4. .Vurgafman, J.R. Meyer, L.R.Ram-Mahan, IEEE Photonic Technol. Lett. 9, 170 (1997)
5. A.Popov, V.Sherstnev, Yu.P.Yakovlev, Appl. Phys. Lett 68 (20), 2790, (1996)
6. Z.Feit, D.Kosty, R.J.Woods, P.Mak, Appl. Phys. Lett. 57, 2881 (1990)
7. G.G.Zegrya, A.D.Andreev Appl. Phys. Lett. 67, 2681, (1995)
8. Yu. P. Yakovlev, T.N.Danilova, A.N.Imenkov, M.P.Mikhailova, K.D.Moiseev, V.V.Sherstnev, G.G.Zegrya, SPIE, vol. 3001 (1997)
9. N.A.Gun`ko, V.B.Khalfin, Z.N.Sokolova, G.G.Zegrya, J.Appl.Phys. 84(1), 547-554 (1998)
10. M.P.Mikhailova, D.N.Nasledov, S.V.Slobodchikov, M.Khamrokubov Fizika Tverdogo Tela (Sol. Solid-State Physics), 15, 390, (1973)
11. G.N.Galkin, F.F.Kharakorin, E.V.Shatkovsky, Fiz. Techn. Poluprov. (Sov. Phys. Semicond.) 5, 442, (1971)
12. D.Z.Garbuzov, M.R.Cokhale, J.C.Dries, P.Studenkov, R.V. Martinelly, J.C.Connolly and S.R.Forrest, Electronics Letters 33, 17, 1462-1465, 1997
13. K.D.Moiseev, M.P.Mikhailova, O.G.Ershov, Yu.P.Yakovlev Semiconductors 30(6), 223-225(1996)
14. K.D.Moiseev, M.P.Mikhailova, O.G.Ershov, Yu.P.Yakovlev Tech. Phys. Lett. 23(2), 151-153
15. A.Krier, H.Gao, V.Sherstnev, Yu.Yakovlev J.Phys.D.-Appl.Phys. 32(24), 3117-3121 (1999)

16. T.N.Danilova, O.G.Ershov, A.N.Imenkov, M.V.Stepanov, V.V.Sherstnev, Yu.P.Yakovlev Semiconductors 30(7), 667-670(1996)

17. M.Aidaraliev, N.V.Zotova, S.A.Karandashev, N.M.Stus, G.N.Talalakin Semiconductors 33(2), 200-205 (1999)

18. S.Ivanov aand P.Kop`ev, Type-II (AlGa)Sb/InAs Quantum Well Structures and Superlattices for Opto-and Microelectronics Grown by Molecular Beam Epitaxy, Chapter 4, in vol. 3 "Antimonide-Related Strained-Layer Heterostructures" Ed. By M.O.Manasreh, in Ser. "Optoelectronic Properties of Semiconductors and Superlattices" (Gordon & Breach Science Publishers, 1997), pp. 95-170.

19. P.V.Necliudov, S.V.Ivanov, B.Ya. Meltser, P.S.Kop`ev, Semiconductors 31, 1067 (1997).

20. V.A.Solovjev, M.P.Mikhailova, M.V.Stepanov, V.V. Sherstnev, Semiconductors 32 (11), 1157-1161, 1998.

21. T.N.Danilova, O.G.Ershov, A.N.Imenkov, M.V.Stepanov, V.V.Sherstnev, Yu.P.Yakovlev Semiconductors 30 (7), 667-670 (1996).

22. N.K.Choi, G.W.Turner, M.J.Manfra, Electron. Lett. 32(14), 1296 (1996).

23. W.W.Bewley, H.Lee, I. Vurgaftman, R.J.Menna, C.L.Felix, R.U.Martinelli, D.W.Stokes, D.Z.Garbuzov, J.R.Meyer, M.Maiorov, J.C.Connolly, A.R.Sugg, G.H.Olsen, Appl. Phys. Lett., 76(3) 256 (1999)

24. J. Faist, F. Capasso, D.L. Sivco, A.L. Hutchinson, S.G. Chu, A.Y. Cho, Appl. Phys. Lett., 72(6), 680 (1998).

25. Kunishige Oe, Koichi Sugiyama, Appl. Phys. Lett., 33(5), 449 (1978).

26. Kressel H., Nelson H., "Properties and Applications of III-V Compound films Deposited by Liquid Phase Epitaxy",- In : Phys of thin films, v.7, New York-London, Academic Press, 1973, p.362

27. M.Aidaraliev, N.V..Zotova, S.A.Karandashov, B.A. Matveev, M.A.Remennyi, N.M.Stus', G.N. Talalakin, T. Beyer*. Semiconductors, v.34, No7 (2000)

28. N.V..Zotova, S.A Karandashov, B.A. Matveev, M.A.Remennyi, N.M.Stus' and G.N. Talalakin, "Gadolinium -doped InGaAsSb solid solutions on an InAs substrate for light-emitting diodes operating in the spectral interval λ=3-5 μm", Semiconductors, vol.33(1999), No 8, pp. 920-923

29. K.D.Moiseev, M.P.Mikhailova, O.G.Ershov, Yu.P. Yakovlev, Tech. Phys. Lett. 21, 482-485 (1995)

30. K.D.Moiseev, M.P.Mikhailova, O.G.Ershov, Yu.P. Yakovlev, Tech. Phys. Lett. 23, (2), 151-153 (1997)

31. M.P.Mikhailova , B.E.Zhurtanov, K.D. Moiseev, A.N. Imenkov, O.G.Ershov, Yu.P. Yakovlev MRS Fall Meeting Proc. Vol. 484, 101-106 (1998).

32. M.P.Mikhailova, K.D. Moiseev, G.G. Zegrya, Yu.P. Yakovlev, Sol. St. Electr., 40, n 1/8, 673-677 (1996).

33. K.D. Moiseev, B.Ya. Meltzer, V.A. Solov`ev, M.P. Mikhailova, S.V. Ivanov, Yu.P. Yakovlev, P.S. Kop`ev, Techn. Phys. Lett. 24 (6) 477-479 (1998).

34. S.V.Ivanov, K.D. Moiseev, A.M.Monakhov, I.V.Sedova, V.A.Solojev, M.P.Mikhailova, Ya.V.Terentyev, B.Ya.meltzer, A.A.Toropov, Yu.P.Yakovlev and P.S. Kopjev, Proc. Intern. Conf. Nanostructures: Physics and Technology St.Petersburg, June 2000, p. 109-112.

35. S.V. Ivanov, S.V.Sorokin, P.S. Kop'ev, J.R. Kim, H.D. Jung and H.S. Park, J. Cryst. Growth 159, 16 (1996)

36. S.V. Ivanov, S.V. Sorokin, I.L. Krestnikov, N.N. Faleev, B.Ya. Ber, I.V. Sedova, and P.S. Kop'ev, J. Cryst. Growth 184/185, 70 (1998)

37. C.G. Van de Walle, Phys B 39, 1871 (1989).

Publications in the frame of this Contract

1.* Yu.P.Yakovlev, K.D.Moiseev, M.P.Mikhailova, A.P.Danilova "High-power mid-infrared lasers based on type II heterostructures with asymmetric band offset confinement" Abstracts of MIOMD-III Aachen, Germany, 5-7 September, 1999, P-18

2.* M.P.Mikhailova, B.E.Zhurtanov, K.D. Moiseev, N.D.Stoyanov, Yu.P.Yakovlev "Bistability and blue shift of electroluminescence in typeII asymmetric AlGaAsSb/InGaAsSb double heterostructures" Abstracts of MIOMD-III Aachen, Germany, 5-7 September, 1999, P-12.

3.* Yu.P.Yakovlev "High-power mid-infrared lasers based on type II heterostructures with asymmetric band offset confinement" SPIE vol. 3947, p.144-153, 2000.

4.* S.V.Ivanov, K.D. Moiseev, A.M.Monakhov, I.V.Sedova, V.A.Solov`ev, M.P.Mikhailova, Ya.V.Terentyev, B.Ya. Metzer, A.A.Toropov, Yu.P.Yakovlev, and P.S.kopjev. "Electroluminescence properties of a new asymmetric AlSbAs/InAs/II-VI double heterostructures grown by MBE" Proc. Of the Int. Conf. Nanostructure: Physics and Technology, St.Petersburg, Russia June 2000, p. 109-112.

5.* Ya.V.Terent`ev, A.A.Toropov, B.Ya.Meltzer, V.A.Solov`ev, S.V.Ivanov, P.S.Kop`ev, B.Magnusson, B. Monemar Photoluminescence studies of InAs/InSb nanostructures grown by MBE Proc. Of 8th Int. Symp. "Nanostructures: Physics and Technology", St. Petersburg, Russia, June 19-23, 2000, p. 145-147.

6.* V.A.Solov`ev, K.D.Moiseev, I.V.Sedova, Ya.V.Terent`ev, M.P.Mikhailova, A.M.Monakhov, B.Ya.Meltzer, P.S.Kop`ev MID-IR LED based on a new asymmetric p-AlSbAs/i-InAs/n-(Mg,Cd)Se double heterostructure Laser Optics-2000 26-30 June 2000, St.Petersburg

7.* M.Aidaraliev, N.V..Zotova, S.A.Karandashov, B.A. Matveev, M.A.Remennyi, N.M.Stus', G.N. Talalakin , T. Beyer and R. Brunner «Spectral Characteristics of Lasers Based on InGaAsSb/InAsSbP Double Heterostructures (λ=3.0÷3.6 μm)», Semiconductors, Vol.34, No4, 2000, pp.488-492

8.* M.Aidaraliev, N.V..Zotova, S.A.Karandashov, B.A. Matveev, M.A.Remennyi, N.M.Stus', G.N. Talalakin, T. Beyer*. Semiconductors, v.34, No 7 (2000)

9.* N.V.Zotova, N.Il'inskaya, S.V.Karandashov, B.A.Matveev, M.Remennyi, N.M.Stus', G.N.Talalakin, M.Aydaraliev, V.Shustov "DH InGaAsSb(Gd)/InAsSbP (λ≅3.3μm) High Power Diode Lasers", *to be submitted to Semiconductors in July, 2000*

10.* T.N.Danilova, A.N.Imenkov, V.V.Sherstnev, Yu.P.Yakovlev "InAsSb/InAsSbP DH lasers for the spectral range 3-4 μm" Semiconductors, 34, 11 (2000).

12. Delivery list

Final report is presented as a result of the one-year work under the Contract. Three samples of the broad-stripe lasers demonstrating high output power in cw mode and pulsed mode are fabricated and will be delivered. Three samples of LED-2 structures based on InAs/GaSb MQWs are also prepared and ready to delivery.